Fractional Modeling of MHD Casson Flow with Heat and Mass Transfer in a Porous Medium Using the Constant-Proportional Caputo Derivative

This work is licensed under a Creative Commons Attribution 4.0 International License

M. Kazim,[a] M. A. Abbas,[a] M. M. Bhatti,[b,c,d,*] O. A. Bég,[e] and T. A. Bég[f]

[a]Department of Mathematics, University of Baltistan, Skardu 16300, Pakistan

[b]Department of Physics, College of Science, Korea University, 145 Anam-ro, Seongbuk-gu, Seoul 02841, Republic of Korea

[c]Jadara University Research Center, Jadara University, Jordan

[d]Department of Mathematics and Natural Sciences, Center for Applied Mathematics and Bioinformatics (CAMB), Gulf University for Science and Technology, 32093 Hawally, Kuwait

[e]Multi-Physical Engineering Sciences Group, Dept. Mechanical and Aeronautical Engineering, Corrosion/Coatings Lab, 3-08, SEE Building, Salford University, Manchester, UK

[f]Engineering Mechanics Research, Israfil House, Dickenson Rd., Manchester, M13, UK

doi: https://doi.org/10.15255/CABEQ.2026.2562

Original scientific paper
Received: July 16, 2026
Accepted: October 8, 2026

In this study we developed a new model of fractional magnetohydrodynamic (MHD) polymeric Casson flow, heat and mass transfer from a wall adjacent to a porous medium with viscous dissipation, heat generation and activation energy effects, a problem of relevance to non-Newtonian functional thermal materials processing and smart lubricant manufacturing. Fractional derivatives were used to extend the Casson viscoplastic model (which featured shear-thinning and yield stress effects) in order to represent complex non-Newtonian responses and memory-dependent behaviour. The mathematical formulation was developed using a newly suggested constant-proportional Caputo fractional derivative (CPCFD). The transformed dimensionless fractional governing equations for mass, momentum, energy and species concentration were solved via Laplace integral transform technique (LITT), under suitable boundary conditions. MATHCAD software was used to evaluate solutions for non-dimensional velocity, $\mathcal{U}$ temperature, $\mathcal{T}$ and concentration, C, with variation in transverse coordinate ψ and time t. Nusselt number, Sherwood number and skin friction solutions are also presented. The impact of key emerging parameters on these variables was examined. Verification with previous studies neglecting porous media, magnetic field, heat generation, activation energy and viscous heating effects is also included. An increase in activation energy parameter (E_a), i.e., minimum energy threshold required for a chemical reaction to occur, reduces considerably species concentrations. Skin friction, Nusselt number, and Sherwood number were reduced with increasing fractional parameter (α) but increased with time (t). A higher Damköhler number (D_v) increased the dominance of the reaction, increasing species consumption and decreasing concentration. An elevation in fractional derivative parameter (γ) improved the system memory effects, suppressed mass diffusion and reduced concentration magnitudes. Fractional calculus enables engineers to define the memory and non-local hereditary effects of polymer chains. Higher Schmidt number (Sc) depleted species diffusion and concentration boundary-layer thickness. Increasing Eckert number (Ec, viscous heating parameter) boosted temperature magnitudes whereas higher permeability parameter reduced them. Higher values of Casson rheological parameter (σ) decelerated the flow and increased momentum boundary-layer thickness. An upsurge in magnetic parameter (Ha, i.e., stronger magnetic field intensity and Lorentzian magnetohydrodynamic drag) strongly dampened the flow. Temperature significantly increased with greater heat generation parameter (δ). These findings may be beneficial to more sophisticated simulation of industrial viscoplastic functional coating systems. Future work may explore extensions to non-Fourier heat conduction, non-Darcy media, and consider periodic boundary conditions.

Keywords

Casson non-Newtonian polymer, constant-proportional Caputo fractional derivative (CPCFD) formulation, activation energy, heat generation, Laplace integral transform technique (LITT), Damköhler number

*Corresponding author: Email: mmbhatti@sdust.edu.cn

Introduction

Non-Newtonian fluids exhibit nonlinear relationships between the shear strain rate and shear stress and due to their complex behavior. This produces strong nonlinearity in mathematical models. Simulation of non-Newtonian fluids is of great interest in multiple technological sectors including foams, emulsions, colloids, gels, pastes, and suspensions, pharmaceutics, cosmetics, food processing etc.[1] Among the many types of rheological fluids, viscoplastic fluids are especially of interest in coating flows[2]. Such fluids require a minimum stress threshold (the yield stress) to start moving. Common in dense suspensions, foams, and gels, these complex fluids flow like liquids when stressed, but behave as unyielded, solid-like "plugs" when stresses fall below the yield limit. A variety of models are available for studying viscoplastic flows, including the Bingham Plastic Model, which is the most elementary and assumes the polymer acts as a rigid solid until the yield stress is attained, after which it flows with a constant, linear viscosity[3]. The Herschel–Bulkley Model is more advanced, and it combines power-law behavior with yield stress (Bingham plastic) effects. It accounts for shear-thinning (or shear-thickening) behavior after yielding occurs, and is dependent on a rheological behavior index[4]. A more comprehensive model is the Casson Model, which is very popular for the food and biomedical coating sectors and simulates polymeric materials with pronounced yield stress and varying viscosity at higher shear rates[5]. In recent years, this model has been deployed extensively for coating flows with heat and mass transfer. In many such studies, which compliment laboratory rheological testing, nonlinearity of the conservation equations requires powerful numerical or analytical techniques to yield robust solutions[6]. Kumar *et al.*[7] used a finite difference computational method to study Casson thermo-solutal convective transport from a vertical porous boundary with radiative flux and cross diffusion effects. They noted that increasing Casson parameter strongly dampens velocity and increases momentum boundary layer thickness, while both velocity and concentration increase with the Soret thermos-diffusion parameter. They also reported that the momentum and thermal boundary-layer thickness increase with increasing Dufour number. Shahidi *et al*.[8] employed an efficient Chebyshev Spectral Newton Iterative Scheme (CSNIS), implemented in MATLAB, to compute the laminar viscoplastic boundary-layer flow and mixed-convective heat transfer over a power-law nonlinear stretching surface using the non-Fourier hyperbolic Cattaneo-Christov heat flux model and Rosseland radiative algebraic flux model. They noted that an increment in Casson viscoplastic parameter reduces both velocity and the Nusselt number but increases temperature. They further observed that higher values of the non-Fourier Deborah number decrease temperatures, whereas increasing the radiative flux parameter increases temperature.

Magnetic fluid coatings are advanced functional materials that provide enhanced protection and tunability for substrates (coated components), and interact with external magnetic fields, enabling friction-reducing lubrication and smart response to varying environmental conditions. They are suspensions composed of magnetic particles, surfactants, and non-magnetic carrier liquids. Magnetic fluids are widely used in various fields, including surface deposition and sealing, due to their excellent and rapid magnetic response, flexible flow ability, tunable magneto-viscous effect, and reliable self-repairing capability. They include ferrofluids, magnetic-receptive paints and electro-conductive polymers. Magnetic viscoplastic coatings are a subset of magnetic polymers that combine viscoplastic behaviour and magnetohydrodynamic (MHD) or ferromagnetic characteristics. As such, they are advanced, multi-responsive materials. When subjected to an external magnetic field, they undergo controlled, reversible transitions in physical properties, including viscosity modification, stiffness, and fluidity (viscoplasticity) within milliseconds. These functional polymers are increasingly being used for coating systems in advanced actuation, soft robotics and artificial muscles where controlled shape morphing is required, and numerous other areas, including structural dynamic (vibration) control and fuel cell coatings[9,10]. A number of researchers have investigated viscoplastic MHD coating flows using the robust Casson model. Kausar *et al.*[11] used MATLAB bvp4c algorithms to simulate Casson magnetized coating boundary-layer transport along a vertically extending perforated surface (substrate) embedded in a porous matrix incorporating nanoparticle, bioconvective, thermal radiation, and heat generation effects. They noted that stronger wall-injection and buoyancy-force-ratio parameters accelerate the flow, whereas the opposite effect was observed with increasing permeability, Casson viscoplastic, magnetic, suction, and bioconvection Rayleigh parameters. Sowmiya *et al.*[12] employed a Laplace transform technique (LTT) and MATLAB software to analyze the magnetized free convective thermo-solutal Casson viscoplastic transport from a rotating vertical wall in a permeable medium with ramped wall temperature. They observed that higher values of magnetic, Casson, and rotational parameters all suppress velocity, and that ramped wall temperature increases momentum boundary layer thickness relative to the isothermal wall case. Fur-

ther studies include Vasu *et al.*[13] (who used a homotopy and generalized differential quadrature numerical method to compute time-dependent nano-bioconvection flow of a magnetic Casson coating along a stretching sheet: HAM and GDQ computation), Nasir *et al.*[14] (on Ohmic dissipation, wall slip and thermal/solutal stratification effects in hydromagnetic Casson stretching flow adjacent to a porous medium), and Sreenivasulu *et al.*[15] (on Casson hybrid nanofluid polymeric coating flow of a cylinder with hydrodynamic and thermal slip and radiative heat transfer). All these investigations confirmed the substantial modification in momentum, thermal and/or species concentration characteristics with Casson yield stress effects, and strong deviation from classical Newtonian models.

Chemical reactions in polymer coating flows involve complex interactions between fluid dynamics and reactive chemistry. They drive crucial processes wherein the polymer liquid resin mixtures must spread evenly before reacting to form a solid, durable film (coating)[16]. As chemical reactions progress, the molecular weight of the polymer increases exponentially, leading to a drastic rise in viscosity. This is especially important in emulsion polymerization[17]. Mathematical flow models require detailed assessment of solutal (mass) diffusion with chemical reactions to simulate these processes. In addition, non-Newtonian effects can be present. Fick's law of mass (species) diffusion is usually adopted when solutal relaxation effects are neglected[18]. Flow shear stresses can stretch polymer chains. If mechanical forces overcome the local thermal activation energy barrier, they may trigger targeted bond scission and chemical changes within the flowing material[19]. The Arrhenius model is a popular model for studying activation energy effects on reactive polymer dynamics. It quantifies how the rate of a chemical reaction or molecular degradation accelerates as temperature increases. It assumes that reaction rate constantly increases exponentially with the absolute temperature governed by a specific energy barrier called the activation energy. It therefore mathematically defines how chemical reaction rates scale exponentially with absolute temperature, depending directly on the activation energy required for the molecules to react, and is very popular in a range of polymer processing applications, including assessing corrosion rates under accelerated heat conditions, magneto-chemical techniques, etc. Several researchers have explored this model in the context of Casson polymeric reactive coating flows. Reddy *et al.*[21] computed the combined effects of Dufour cross diffusion, slip, activation energy, and magnetic field on Casson polymer flow along a stretching permeable wall with suction/injection. They demonstrated that Sherwood number (mass transfer rate) is depleted with stronger activation energy parameter, larger Dufour effect increases thermal gradients, whereas stronger magnetic field and Casson parameter inhibit flow. Aarathi *et al.*[22] computed the thermal solutal unsteady reactive magnetized non-Newtonian micropolar nanofluid transport along an inclined stretched surface with activation energy and entropy generation effects using a fourth-order Runge-Kutta scheme combined with a shooting technique. They noted that increasing activation energy strongly boosts nanoparticle concentration, whereas an increase in binary chemical reaction produces a reduction. They further noted that increasing the unsteadiness parameter raises the skin-friction coefficient by more than 50 %, while stronger viscous dissipation and Casson viscoplastic effects increase the rate of entropy generation. Further studies include Prabu *et al.*[23] (on non-Fourier and thermos-capillary effects in Casson flows), and Zhang *et al.*[24] (on spectral computation of magnetized nanofluid boundary-layer flow in porous media). Significant modifications in velocity, temperature, and species concentration characteristics with increasing activation and chemical reaction rate effects have been confirmed in all these studies.

The models previously discussed employed conventional integer-order calculus in formulations. However, fractional calculus extends differentiation and integration to non-integer or complex orders and enables better experimental fitting with actual nonlinear polymeric flows. The theory of fractional calculus encompasses old calculus, extending the ideas of derivatives and integrals to fractional cases. Although ordinary derivatives include differentiation with integer exponents, fractional derivatives join fractional or real-order derivatives. These are suitable for describing more complex methods that depend on memory and cannot be exactly represented using only integer-order calculus. As such, fraction calculus has emerged as a major subsection of modern mathematics and has stimulated rich development in multiple formulations for fractional derivatives and integrals that provide a more realistic analysis of real-world physics. Fractional derivatives have been used to study a range of physical models in a number of scientific fields. They make it easier to create more accurate models in a variety of fields, specifically in physical structures with long-term memory or inherited characteristics. They have attracted interest due to their capacity to depict phenomena such as inconsistent diffusion, viscoelasticity, viscoplasticity, and fractal dynamics. In mathematics, fractional derivatives are notably used to model irregular diffusion processes, where the rate of variation is not constant but changes with time. The Caputo time fractional derivative method

is a foundational tool in fractional calculus, introduced by Italian mathematician and geophysicist, Michele Caputo, in 1967. It is primarily used to model anomalous diffusion, viscoelasticity, and systems with "memory" because it directly incorporates conventional, physically meaningful initial and boundary conditions. This approach has been employed in a number of studies in Casson viscoplastic fluid dynamics in recent years. Nadeem *et al.*[25] investigated the time-dependent thermal convection flow of a magnetic non-Newtonian fractional Casson fluid. They employed Caputo's fractional derivatives account for hereditary and relaxation polymer properties and derived closed-form solutions with Fourier and Fourier sine transforms. They noted that elevation in fractional parameter accelerates the flow, whereas larger Strouhal numbers result in sharper velocity peaks and more dominant oscillatory effects on shorter spatial or temporal scales. They also observed that with decreasing Casson parameter, the velocity peaks are accentuated, indicating lower deformation resistance and shear thinning behavior. Alwuthaynani *et al.*[26] investigated non-Fourier and non-Fickian fractional Casson viscoplastic thermal solutal flow with Caputo time-fractional derivatives. They derived analytical solutions for velocity, temperature, and concentration profiles using a combined Laplace–Fourier sine transform technique and noted that fractional-order modelling predicts higher heat transfer rates but lower mass transfer efficiency compared with the classical non-fractional case. The Caputo fractional derivative has also been utilized in other mass diffusion and non-Newtonian studies including oxygen diffusion in rheological blood by Srivastava *et al.*[27], nanoparticle doped electrokinetic viscoelastic stenotic arterial blood flow by Channakote *et al.*[28], and peristaltic viscoelastic pumping in inclined conduits with gravitational effects by Tripathi and Bég[29]. Recent developments in fractional calculus modelling have introduced novel hybrid fractional derivative operators (such as the non-singular exponential-kernel Yang-Abdel-Cattani (YAC) or Constant Proportional Caputo operators) to describe fluid dynamics more accurately. Caputo-Fabrizio (CF) fractional derivatives are an additional formulation of fractional calculus, which unlike classical fractional definitions (like Riemann-Liouville or standard Caputo), rely on singular power-law kernels, the CF derivative utilizes a non-singular exponential kernel. Rehman *et al*.[30] implemented the constant proportional Caputo fractional derivative (CPCFD) operator with non-local and singular kernels in Casson viscoplastic heat transfer along a vertical plate. They derived exact solutions for dimensionless velocity, concentration and energy equations are calculated in terms of Mittag-Leffler functions by employing the Laplace transformation method. They showed that increasing values of the constant proportional Caputo fractional parameter induce a deceleration in the flow and a strong cooling effect. Further studies with modified fractional derivatives include Ahmad *et al.*[31] (who employed the constant proportional Caputo fractional derivative (CPCFD) operator for Maxwell viscoelastic magnetic slip flow, heat and mass transfer), Ali *et al.*[32] (who considered the Atangana-Baleanu (ABC) fractional derivative for micropolar thermo-solutal bioconvection), Jamil *et al.*[33] (on Caputo-Fabrizio fractional derivative modelling of Casson blood flow in inclined vessels), Tabi *et al.*[34] and Abbas *et al.*[35].

A review of the literature indicates that Casson unsteady polymeric reactive thermo-solutal magnetic flow in porous media with viscous heating and Arrhenius chemical kinetics, has not yet been investigated in the technical literature. The present study addresses this problem using a Darcy-type porous drag force model[36–39]. Viscous heating is known to be significant in non-Newtonian polymers flows[40–44]. The analysis further incorporates the effects of the Damköhler number[45]. In the context of polymer coatings, the Damköhler number determines whether a coating process (or its final performance) is kinetically controlled or diffusion- limited[46,47]. Heat generation effects were also incorporated into the mathematical model and are important in thermal treatment of non-Newtonian polymers[48–50]. A generalized formulation in fractional form of Casson magnetic polymer flow using a new fractional operator, the constant-proportional Caputo fractional derivative (CPCFD), with a non-local and singular kernel was developed. Fractional forms of the momentum, energy, and reactive species (concentration) equations were derived subject to appropriate boundary conditions. Therefore, this study generalizes existing studies to explore, for the first time, a broader multi-physical perspective by simultaneously addressing fraction Casson yield stress rheology, viscous dissipation, heat generation, Darcian permeable media impedance, Arrhenius kinetics, polymer reactions and time-dependent behaviour. The transformed dimensionless fractional governing equations for mass, momentum, energy and species concentration were solved using the Laplace integral transformation technique, subject to appropriate boundary conditions. MATHCAD software was used to evaluate solutions for non-dimensional velocity, $\mathcal{U}$ temperature, $\mathcal{T}$ and concentration, C, with variation in transverse coordinate ψ and time t. Nusselt number, Sherwood number, and skin friction solutions are also presented. The impact of key emerging parameters on these variables was examined. Verification with previous studies neglecting

porous media, magnetic field, heat generation, activation energy, and viscous heating effects were included. Key objectives of the current study are summarized below:

– To formulate a novel fractional viscoplastic Casson transport model with the constant-proportional Caputo fractional derivative (CPCFD) formulation.
– To solve the emerging dimensionless system with Laplace integral transformation technique and visualize results graphically with MATHCAD software.
– To elucidate the sensitivity of transport characteristics to CPCFD parameters relative to classical Casson fluid behavior.
– To investigate the impact of non-integer parameter and porous medium (Darcian) drag on heat, mass and momentum characteristics.
– To evaluate the effect of viscous dissipation and heat generation on transport variables.
– To compute and explain the influence of fractional, Schmidt number, and activation energy parameters on mass diffusion.
– To examine the impact of magnetic field on wall characteristics, e.g., Nusselt number.
– To compute the modification in skin friction, Nusselt and Sherwood number with Casson viscoplastic parameter.

Mathematical model

The unsteady, incompressible flow, heat and mass transfer in an electrically conducting Casson polymer along a horizontal surface adjacent to an isotropic, homogenous, non-deformable porous medium was investigated. Heat generation, viscous dissipation, and chemical reaction with activation energy, were all incorporated into the model. Hall current and magnetic induction effects were neglected, as were thermal dispersion and cross diffusion (Soret/Dufour) effects. The physical model is shown in Fig. 1. The following fundamental assumptions were adopted:

– The flow is unidirectional.
– A magnetic field with strength B_0 is applied transverse to the plate (surface).
– Activation energy (Arrhenius kinetics) is incorporated into the concentration equation.
– Classical Fourier heat conduction and Fickian mass diffusion are adopted in the present formulation; consequently, non-Fourier thermal relaxation and finite-speed heat propagation are not represented and are reserved for future extensions.
– The energy equation incorporates the viscous dissipation term and general heat generation.
– Low Reynolds number is prevalent, and the Darcy model is used for porous medium drag.

A Cartesian coordinate ($\mathcal{X}$,ψ) system is adopted. The Cauchy stress tensor for the Casson viscoplastic polymer following Rehman *et al.*[30] takes the form:

$$\tau_{ij}^{*}=\begin{Bmatrix} 2\left(\mu_t+\dfrac{P_\partial}{\sqrt{2\pi}}\right)e_{ij}, & \pi>\pi_z \\ 2\left(\mu_t+\dfrac{P_\partial}{\sqrt{2\pi_z}}\right)e_{ij}, & \pi\le\pi_z \end{Bmatrix} \tag{1}$$

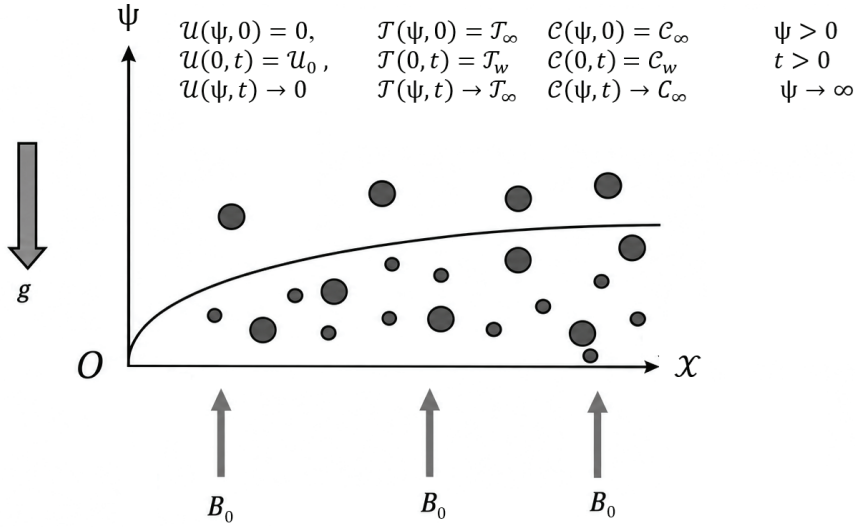


Fig. 1 – *Physical model for magnetic Casson polymer thermo-solutal flow*

where μ_t is the plastic dynamic viscosity, P_∂ is the polymer yield stress, π is the self-product of the deformation rate, e_{ij} is the components of the strain-rate tensor (rate-of-deformation tensor), $\pi = e_{ij}\, e_{ij}$ denotes the second invariant of the rate-of-deformation tensor, π_z is the critical strain-rate invariant e_{ij} which depends upon the non-Newtonian model. The Casson fluid and the solid plate are initially at rest at $t = 0$, with a temperature of $\mathcal{T}_\infty$ and a concentration of $\mathcal{C}_\infty$. Subsequently, when time is $t = 0^+$, the concentration is $\mathcal{C}(0,t) = \mathcal{C}_w$, and the wall temperature is $\mathcal{T}(0,t) = \mathcal{T}_w$. The velocity in the $\mathcal{X}$-direction is $\mathcal{U}$. $\mathcal{U}_0$ is characteristic velocity. Using the above assumptions, the governing conservation equations generalized by extending previous models[51,52] to include Arrhenius kinetics, Darcy, heat generation[60], viscous heating and magnetic body force effects may be shown to take the form:

$$\nabla \cdot V = 0 \tag{2}$$

$$\frac{\partial \mathcal{U}(\psi,t)}{\partial \mathcal{X}} + \frac{\partial v(\psi,t)}{\partial \psi} = 0 \tag{3}$$

$$\frac{\partial \mathcal{U}(\psi,t)}{\partial t} = v\left(1+\frac{1}{s}\right)\frac{\partial^2 \mathcal{U}(\psi,t)}{\partial \psi^2} - \frac{\mu\varphi}{\rho k_1}\mathcal{U}(\psi,t) - \frac{\sigma {B_0}^2}{\rho}\mathcal{U}(\psi,t) \tag{4}$$

$$\rho C_p \frac{\partial \mathcal{T}(\psi,t)}{\partial t} = k\frac{\partial^2 \mathcal{T}(\psi,t)}{\partial \psi^2} + \left(1+\frac{1}{s}\right)\Phi + Q_0\left(\mathcal{T}-\mathcal{T}_\infty\right) \tag{5}$$

$$\frac{\partial \mathcal{C}(\psi,t)}{\partial t} = D\frac{\partial^2 \mathcal{C}(\psi,t)}{\partial \psi^2} + k_0\left(\mathcal{C}-\mathcal{C}_\infty\right)\exp\left(-\frac{E_a}{R\mathcal{T}}\right) \tag{6}$$

where Φ is viscous dissipation,

$$\Phi = \mu\left[2\left(\left(\frac{\partial \mathcal{U}}{\partial \mathcal{X}}\right)^2 + \left(\frac{\partial v}{\partial \psi}\right)^2\right) + \left(\frac{\partial \mathcal{U}}{\partial \psi} + \frac{\partial v}{\partial \mathcal{X}}\right)^2\right].$$

The following initial conditions and boundary conditions are prescribed:

$$\begin{aligned} &\mathcal{U}(\psi,0) = 0,\ \ \mathcal{T}(\psi,0) = \mathcal{T}_\infty,\ \ \mathcal{C}(\psi,0) = \mathcal{C}_\infty,\ \ \psi > 0 \\ &\mathcal{U}(0,t) = \mathcal{U}_0,\ \ \mathcal{T}(0,t) = \mathcal{T}_w,\ \ \ \mathcal{C}(0,t) = \mathcal{C}_w,\ \ \ t > 0 \\ &\mathcal{U}(\psi,t) \to 0,\ \ \mathcal{T}(\psi,t) \to \mathcal{T}_\infty,\ \ \mathcal{C}(\psi,t) \to \mathcal{C}_\infty,\ \text{as}\ \psi \to \infty \end{aligned} \tag{7}$$

The boundary conditions determine the interface between the wall and the surrounding fluid. The mechanical, thermal, and mass-transfer effects of the surface are represented by the fluid's compliance with the prescribed wall velocity, wall temperature, and wall concentration $\psi = 0$. Whereas, the velocity approaches zero, and the concentration and temperature, $\mathcal{T}_\infty$ and $\mathcal{C}_\infty$, respectively, approach their ambient values. As a result, it is assumed that the wall's effects disappear sufficiently far below the surface.

To facilitate analytical solutions, the following non-dimensional variables are invoked:

$$\begin{aligned} &t^{\mathfrak{H}} = \frac{{\mathcal{U}_0}^2 t}{v},\quad \psi^{\mathfrak{H}} = \frac{\mathcal{U}_0 \psi}{v},\quad \mathcal{U}^{\mathfrak{H}} = \frac{\mathcal{U}}{\mathcal{U}_0},\quad \mathcal{C}^{\mathfrak{H}} = \frac{\mathcal{C}-\mathcal{C}_\infty}{\mathcal{C}_w-\mathcal{C}_\infty}, \\ &\mathcal{T}^{\mathfrak{H}} = \frac{\mathcal{T}-\mathcal{T}_\infty}{\mathcal{T}_w-\mathcal{T}_\infty},\quad K = \frac{v^2\varphi}{{u_0}^2 k_1},\quad \mathrm{Ha}^2 = \frac{\sigma {B_0}^2 v}{\rho {u_0}^2}, \\ &\lambda = 1+\frac{1}{s},\quad Pr = \frac{\mu C_p}{k},\quad \mathrm{Ec} = \frac{{u_0}^2}{C_p \Delta\mathcal{T}},\quad \delta = \frac{Q_0 v}{\rho C_p {u_0}^2}, \\ &\mathrm{Sc} = \frac{v}{D},\quad D_v = \frac{k_0 v}{{u_0}^2},\quad E = \frac{E_a}{R\mathcal{T}_\infty},\quad \text{ч} = \frac{\mathcal{T}^{\mathfrak{H}}\left(\mathcal{T}_w-\mathcal{T}_\infty\right)}{\mathcal{T}_\infty} \end{aligned} \tag{8}$$

The advantages of utilizing dimensionless parameters are threesome. Firstly, the model can be rendered into a form in which special cases can be benchmarked directly to the literature, since the majority of studies published also use this approach. Secondly, the need for explicit material or geometric data is circumvented, since dimensionless numbers provide a methodology of simulating fluid dynamics problems via scaling numbers that embody relative effects of different phenomena, e.g., Prandtl number represents the ratio of momentum to thermal diffusion and while it features specific heat capacity, dynamic viscosity and thermal conductivity, these material properties do not need explicit specification to obtain meaningful solutions to the analysis. This facilitates much faster simulations that remain physically viable. Thirdly, dimensionless numbers decrease the number of independent variables needed to analyze a system, condensing many parameters into fewer ratios. They therefore simplify complex physical systems by grouping multiple dimensional variables into single, unitless ratios, and this is a major reason why this approach has remained popular for over a century in fluid dynamics. They provide a clear physical meaning by showing the relative magnitude of competing forces or rates, e.g., the ratio of convective to conductive heat transfer expressed in the Nusselt number or the ratio of momentum diffusion rate to molecular (mass) diffusion rate as expressed in the Schmidt number. In Eqn. (8) $t^{\mathfrak{H}}$ is dimensionless time, $\psi^{\mathfrak{H}}$ is dimensionless vertical (transverse coordinate), is dimensionless velocity, $\mathcal{C}^{\mathfrak{H}} = \frac{\mathcal{C}-\mathcal{C}_\infty}{\mathcal{C}_w-\mathcal{C}_\infty}$, is dimensionless concentration of reactive species, $\mathcal{T}^{\mathfrak{H}}$ is dimensionless temperature, K is dimension-

less permeability parameter, Ha^2 is the square of the modified Hartmann magnetic number, λ is a function of the Casson viscoplastic parameter (ς), Pr is Prandtl number, Ec is Eckert (viscous heating) number, δ is heat generation (source) parameter, Sc is Schmidt number, D_v is Damköhler number, $E=\frac{E_a}{R\mathcal{T}_\infty}$, is Arrhenius activation energy parameter, $\mu=\frac{\mathcal{T}^{\mathfrak{H}}\left(\mathcal{T}_w-\mathcal{T}_\infty\right)}{\mathcal{T}_\infty}$. By virtue of Eq. (6), the conservation Eqs. (1)–(5) reduce to the following non-dimensional partial differential Eqs., where the superscript $\mathfrak{H}$ is dropped for convenience:

$$\frac{\partial\mathcal{U}(\psi,t)}{\partial t}=\lambda\frac{\partial^2\mathcal{U}(\psi,t)}{\partial\psi^2}-(K+\mathrm{Ha}^2)\mathcal{U}(\psi,t) \quad (9)$$

$$\frac{\partial\mathcal{T}(\psi,t)}{\partial t}=\frac{1}{\mathrm{Pr}}\frac{\partial^2\mathcal{T}(\psi,t)}{\partial\psi^2}+\mathrm{Ec}\lambda\left(\frac{\partial\mathcal{U}(\psi,t)}{\partial t}\right)^2+\delta\mathcal{T} \quad (10)$$

$$\frac{\partial\mathcal{C}(\psi,t)}{\partial t}=\frac{1}{\mathrm{Sc}}\frac{\partial^2\mathcal{C}(\psi,t)}{\partial\psi^2}+D_v\exp\left(-\frac{E}{\mu+1}\right)C \quad (11)$$

Furthermore, the emerging dimensionless initial and boundary conditions (6) become:

$$\mathcal{U}(\psi,0)=0,\ \mathcal{T}(\psi,0)=0,\ \mathcal{C}(\psi,0)=0,\quad \psi>0 \quad (12)$$

$$\mathcal{U}(0,t)=1,\quad \mathcal{T}(\psi,t)=1,\quad \mathcal{C}(0,t)=1,\quad t>0 \quad (13)$$

$$\mathcal{U}(\psi,t)\to 0,\ \mathcal{T}(\psi,t)\to 0,\ \mathcal{C}(\psi,t)\to 0,\ \psi\to\infty \quad (14)$$

Fractional calculus aspects

Baleanu et al.[53] developed a new type of fractional-operator using a power law approach. This was adopted in the present study and is known as the constant-proportional Caputo (CPC) non-integer derivative. It is composed of a linear combination of a constant-proportional operator and a Caputo type fractional technique. In contrast, the traditional Caputo derivative uses a purely fractional integral of the first-order derivative to represent memory effects[61–63]. Therefore, while maintaining the fractional memory effect, replacing the traditional temporal derivative with CPCFD, modifies the time-dependent governing equations by adding an extra proportional component. This formulation allows for a more flexible description of the memory-dependent and inherited behavior of non-Newtonian fluids. The definition of the constant-proportional Caputo type derivative used by Kazim *et al.*[54] is:

$${}^{cpc}D_t^{\gamma}h(r)=\left[\Gamma(1-\gamma)\right]^{-1}\int_0^r\frac{\hbar_1(\gamma)h(\tau)+\hbar_0(\gamma)\dot{h}(\tau)}{(r-\tau)^{\gamma}}d\tau \quad (15)$$

$$0<\gamma<1$$

The Laplace transform formulation for the constant proportional Caputo fractional derivative (CPCFD) is given by:

$$\mathcal{L}\left\{{}^{cpc}D_t^{\gamma}(r)\right\}=\left\{\frac{\hbar_1(\gamma)}{s}+\hbar_0(\gamma)\right\}s^{\gamma}h(s)-\hbar_0(\gamma)s^{\gamma-1}h(0) \quad (16)$$

Here ${}^{cpc}D_t^{\gamma}(\ldots)$ is the constant proportional Caputo hybrid fractional operators, $\hbar_1(\gamma)$ and $\hbar_0(\gamma)$, which simulate fractional characteristics.

Laplace transform solutions

By applying the constant proportional Caputo fractional derivative (CPCFD) operator described in the previous section, the governing conservation equations for momentum, energy and species concentration, Eqs. (8)–(10), are reformulated in fractional form as follows:

$${}^{cpc}D_t^{\gamma}\mathcal{U}(\psi,t)=\lambda\frac{\partial^2\mathcal{U}(\psi,t)}{\partial\psi^2}-(K+\mathrm{Ha}^2)\mathcal{U}(\psi,t) \quad (17)$$

$${}^{cpc}D_t^{\gamma}\mathcal{T}(\psi,t)=\frac{1}{\mathrm{Pr}}\frac{\partial^2\mathcal{T}(\psi,t)}{\partial\psi^2}+\mathrm{Ec}\lambda\left(\frac{\partial\mathcal{U}(\psi,t)}{\partial t}\right)^2+\delta\mathcal{T} \quad (18)$$

$${}^{cpc}D_t^{\gamma}\mathcal{C}(\psi,t)=\frac{1}{\mathrm{Sc}}\frac{\partial^2\mathcal{C}(\psi,t)}{\partial\psi^2}+D_{av}\exp\left(-\frac{E}{\mu+1}\right)\mathcal{C}(\psi,t) \quad (19)$$

We next apply the Laplace transformations to each of these equations. The Laplace transform methodology is restricted to the approximated model developed here. More complex nonlinear 3-D flows would require numerical methods. However, the analytical solutions obtained here provide physically meaningful results and a useful foundation for future, more generalized simulations.

Concentration equation solution and Sherwood number

Applying the Laplace transform technique to Eq. (18), using the initial conditions in Eq. (11), following Yakubu *et al.*[55], yields the following expression:

$$\frac{\partial^2\bar{\mathcal{C}}(\psi,\mathcal{S})}{\partial\psi^2}=\mathrm{Sc}\left[\begin{array}{l}\left\{\frac{\hbar_1(\gamma)}{\mathcal{S}}+\hbar_0(\gamma)\right\}s^{\gamma}\bar{\mathcal{C}}(\psi,\mathcal{S})-\\-\hbar_0(\gamma)\mathcal{S}^{\gamma-1}\bar{\mathcal{C}}(\psi,0)+\\+\frac{D_v e^{\frac{-E}{1+\mu}}}{\mathcal{S}}\bar{\mathcal{C}}(\psi,\mathcal{S})\end{array}\right] \quad (20)$$

$$\bar{\mathcal{C}}(\psi,0)=0,\ \bar{\mathcal{C}}(0,\mathcal{S})=\frac{1}{\mathcal{S}},\ \bar{\mathcal{C}}(\psi,\mathcal{S})\to 0,\ as\ \psi\to\infty \quad (21)$$

The concentration solution, $\bar{\mathcal{C}}(\psi,\mathcal{S})$, is thereby derived using Eqs. (19) and (20) as:

$$\bar{C}(\psi,\mathcal{S})=\frac{1}{\mathcal{S}}e^{-\psi\sqrt{\mathrm{Sc}\left[\left\{\frac{\mathcal{K}_1(\gamma)}{\mathcal{S}}+\mathcal{K}_0(\gamma)\right\}\mathcal{S}^{\gamma}+\frac{D_v e^{\frac{-E}{1+u}}}{\mathcal{S}}\right]}} \tag{22}$$

The inverse Laplace transform can be obtained by rewriting Eq. (21) as follows:

$$\bar{\mathcal{C}}(\psi,\mathcal{S})=\frac{1}{\mathcal{S}}+\sum_{i=1}^{\infty}\sum_{j=0}^{\infty}\sum_{q=0}^{\infty}\frac{(-\psi)^i(\mathrm{Sc})^{\frac{i}{2}}((D_v e^{\frac{-E}{1+u}})^{\frac{i}{2}-j}(\mathcal{K}_1(\gamma))^l}{i!j!q!\mathcal{K}_0(\gamma)^{q-j}\cdot\mathcal{S}^{1+\frac{i}{2}-\gamma j-j+q}}\frac{\Gamma\left(\frac{i}{2}+1\right)\cdot\Gamma(j+1)}{\Gamma\left(1-j+\frac{i}{2}\right)\cdot\Gamma(1-q+j)} \tag{23}$$

By virtue of inverse Laplace transforms, Eq. (22) becomes:

$$\mathcal{C}(\psi,t)=t+\sum_{i=1}^{\infty}\sum_{j=0}^{\infty}\sum_{q=0}^{\infty}\frac{(-\psi)^i(\mathrm{Sc})^{\frac{i}{2}}(D_v.e^{\frac{-E}{1+u}})^{\frac{i}{2}-j}(\mathcal{K}_1(\gamma))^l}{i!j!q!\mathcal{K}_0(\gamma)^{q-j}}\frac{t^{\frac{i}{2}-\gamma j-j+q}\times\Gamma\left(\frac{i}{2}+1\right)\cdot\Gamma(j+1)}{\Gamma\left(1-j+\frac{i}{2}\right).\Gamma(1-q+j)\Gamma(1+\frac{i}{2}-\gamma j-j+q)} \tag{24}$$

Sherwood number (Sh), which represents the dimensionless mass transfer rate at the wall (i.e., ratio of total convective mass transfer to the rate of purely diffusive mass transport), is defined as:

$$\mathrm{Sh}=-\frac{\partial\mathcal{C}(\psi,t)}{\partial\psi}|_{\psi=0} \tag{25}$$

Using inverse Laplace transforms leads to:

$$\mathrm{Sh}=-\frac{\partial}{\partial\psi}\mathcal{L}^{-1}\left\{\mathcal{C}(\psi,\mathcal{S})\right\}|_{\psi=0} \tag{26}$$

This leads to:

$$\mathrm{Sh}=\mathcal{L}^{-1}\left\{\frac{\sqrt{\mathrm{Sc}\left[\left\{\frac{\mathcal{K}_1(\gamma)}{\mathcal{S}}+\mathcal{K}_0(\gamma)\right\}\mathcal{S}^{\gamma}+\frac{D_v e^{\frac{-E}{1+u}}}{\mathcal{S}}\right]}}{\mathcal{S}}\right\} \tag{27}$$

Velocity (momentum) equation solution and skin friction

Applying Laplace transform method to Eq. (16), yields the following eq. with associated initial conditions (11):

$$\frac{\partial^2\bar{\mathcal{U}}(\psi,\mathcal{S})}{\partial\psi^2}=\frac{1}{\lambda}\left[\left\{\frac{\mathcal{K}_1(\gamma)}{\mathcal{S}}+\mathcal{K}_0(\gamma)\right\}\mathcal{S}^{\gamma}\bar{\mathcal{U}}(\psi,\mathcal{S})-\mathcal{K}_0(\gamma)\mathcal{S}^{\gamma-1}\bar{\mathcal{U}}(\psi,0)+\left\{K+\mathrm{Ha}^2\right\}\bar{\mathcal{U}}(\psi,\mathcal{S})\right] \tag{28}$$

$$\bar{\mathcal{U}}(\psi,0)=0,\bar{\mathcal{U}}(0,\mathcal{S})=\frac{1}{s},\bar{\mathcal{U}}(\psi,\mathcal{S})\to 0,\text{ as }\psi\to\infty \tag{29}$$

The solution for the velocity field $\bar{\mathcal{U}}(\psi,\mathcal{S})$ by virtue of Eqs. (27) and (28) is obtained as:

$$\bar{\mathcal{U}}(\psi,\mathcal{S})=\frac{1}{\mathcal{S}}e^{-\psi\sqrt{\frac{1}{\lambda}\left[\left\{\frac{\mathcal{K}_1(\gamma)}{\mathcal{S}}+\mathcal{K}_0(\gamma)\right\}\mathcal{S}^{\gamma}+K+\mathrm{Ha}^2\right)}} \tag{30}$$

Using inverse Laplace transforms on Eqn. (29) yields:

$$\bar{\mathcal{U}}(\psi,\mathcal{S})=\frac{1}{\mathcal{S}}+\sum_{i=1}^{\infty}\sum_{l=0}^{\infty}\sum_{q=0}^{\infty}\frac{(-\psi)^i(\lambda)^{-\frac{i}{2}}((K+\mathrm{Ha})^{\frac{i}{2}-l}(\mathcal{K}_1(\gamma))^q}{i!l!q!\mathcal{K}_0(\gamma)^{q-l}\cdot\mathcal{S}^{1-\gamma l+\mathrm{q}}}\frac{\Gamma(l+1)\cdot\Gamma\left(\frac{i}{2}+1\right)}{\Gamma\left(1-l+\frac{i}{2}\right)\cdot\Gamma(1-q+l)} \tag{31}$$

Using inverse Laplace transforms renders Eqn. (30), as:

$$\mathcal{U}(\psi,t)=t+\sum_{i=1}^{\infty}\sum_{l=0}^{\infty}\sum_{q=0}^{\infty}\frac{(-\psi)^i(\lambda)^{-\frac{i}{2}}(\left(K+\mathrm{Ha}^2\right)^{\frac{i}{2}-l}(\mathcal{K}_1(\gamma)q}{i!l!q!\mathcal{K}_0(\gamma))^{q-l}}\frac{t^{-\gamma l+\mathrm{q}}\times\Gamma\left(\frac{i}{2}+1\right)\cdot\Gamma(l+1)}{\Gamma\left(1-l+\frac{i}{2}\right)\cdot\Gamma(1-q+l)\Gamma(1-\gamma l+\mathrm{q})} \tag{32}$$

Skin friction, (*Cf*), i.e., dimensionless wall shear stress or viscous drag at the interface between the Casson polymer and the wall (skin) is given by:

$$Cf = -\frac{\partial \mathcal{U}(\psi,t)}{\partial \psi}|_{\psi=0} \tag{33}$$

Using inverse Laplace transforms leads to:

$$Cf = -\frac{\partial}{\partial \psi}\mathcal{L}^{-1}\left\{u(\psi,\mathcal{S})\right\}|_{\psi=0} \tag{34}$$

This gives the required result for skin friction:

$$Cf = \mathcal{L}^{-1}\left\{\frac{\sqrt{\frac{1}{\lambda}\left[\left\{\frac{\hbar_1(\gamma)}{\mathcal{S}}+\hbar_0(\gamma)\right\}\mathcal{S}^{\gamma}+K+\mathrm{Ha}^2\right]}}{\mathcal{S}}\right\} \tag{35}$$

Temperature (heat) equation solution and Nusselt number

Finally, Eqn. (17) is converted using the Laplace transform method with initial conditions (11):

$$\frac{\partial^2 \bar{\mathcal{T}}(\psi,\mathcal{S})}{\partial \psi^2} = \mathrm{Pr}\left[\left\{\frac{\hbar_1(\gamma)}{\mathcal{S}}+\hbar_0(\gamma)\right\}\mathcal{S}^{\gamma}\bar{\mathcal{T}}(\psi,\mathcal{S})-\hbar_0(\gamma)\mathcal{S}^{\gamma-1}\bar{\mathcal{T}}(\psi,\mathcal{S})\right]-\frac{\lambda \mathrm{EcPr}A}{\mathcal{S}^2}e^{-2\psi\sqrt{A}}-\delta\mathcal{T} \tag{36}$$

$$\bar{\mathcal{T}}(\psi,0)=0, \bar{\mathcal{T}}(0,\mathcal{S})=\frac{1}{\mathcal{S}}, \bar{\mathcal{T}}(\psi,\mathcal{S})\to 0, \text{as } \psi\to\infty \tag{37}$$

where $A=\frac{1}{\lambda}\left[\left\{\frac{\hbar_1(\gamma)}{\mathcal{S}}+\hbar_0(\gamma)\right\}\mathcal{S}^{\gamma}+K+\mathrm{Ha}^2)\right]$.

The solution for the temperature, $\bar{\mathcal{T}}(\psi,\mathcal{S})$, from Eqs. (35) and (36) is extracted as:

$$\bar{\mathcal{T}}(\psi,\mathcal{S}) = \frac{1}{\mathcal{S}}e^{-\psi\sqrt{\mathrm{Pr}\left[\left\{\frac{\hbar_1(\gamma)}{\mathcal{S}}+\hbar_0(\gamma)\right\}\mathcal{S}^{\gamma}+\delta\right]}}-\frac{\lambda \mathrm{EcPr}A}{\mathcal{S}^2\left(4A-\mathrm{Pr}\left[\left\{\frac{\hbar_1(\gamma)}{\mathcal{S}}+\hbar_0(\gamma)\right\}\mathcal{S}^{\gamma}+\delta\right]\right)}e^{-\psi\sqrt{\mathrm{Pr}\left[\left\{\frac{\hbar_1(\gamma)}{\mathcal{S}}+\hbar_0(\gamma)\right\}\mathcal{S}^{\gamma}+\delta\right]}}+ \tag{38}$$

$$\frac{\lambda \mathrm{EcPr}A}{\mathcal{S}^2\left(4A-\mathrm{Pr}\left[\left\{\frac{\hbar_1(\gamma)}{\mathcal{S}}+\hbar_0(\gamma)\right\}\mathcal{S}^{\gamma}+\delta\right]\right)}e^{-2\psi\sqrt{A}}$$

By applying the inverse Laplace transforms, Eqn. (37) becomes:

$$\bar{\mathcal{T}}(\psi,\mathcal{S}) = \frac{1}{\mathcal{S}}+\sum_{i=1}^{\infty}\sum_{j=0}^{\infty}\sum_{h=0}^{\infty}\frac{(-\psi)^i(Pr)^{\frac{i}{2}}(\delta)^{\frac{i}{2}-j}(\hbar_1(\gamma))^h}{i!j!h!\hbar_0(\gamma))^{h-j}\mathcal{S}^{1-\gamma j+h}}\times\frac{\Gamma(j+1)\Gamma\left(\frac{i}{2}+1\right)}{\Gamma\left(1-j+\frac{i}{2}\right)\Gamma(1+j-\mathrm{k})}-$$

$$\sum_{i=0}^{\infty}\sum_{j=0}^{\infty}\sum_{h=0}^{\infty}\sum_{l=0}^{\infty}\sum_{m=0}^{\infty}\sum_{n}^{i\infty}\sum_{p}^{i\infty}\sum_{q=0}^{\infty}\frac{(-1)^{l+n}(-\psi)^i(Pr)^{1+l+\frac{i}{2}}(\delta)^{\frac{i}{2}-j+l-m}Ec\times\lambda^{l+1}(\hbar_1(\gamma))^{p+q+h}}{4^{1+l}\times h!i!j!p!q!m!n!\times(K+Ha^2)^{l+n}\times\hbar_0(\gamma))^{h-j-\gamma m-n+q+p}\times\mathcal{S}^{2+h-\gamma j-\gamma n-\gamma m+p+q}}\times$$

$$\frac{\Gamma\left(\frac{i}{2}+1\right).\Gamma(j+l)\Gamma(l+1).\Gamma(q+l)\Gamma(m+1)\Gamma(n+l)}{\Gamma(1-j+i).\Gamma(j+1-h)\Gamma(l)\Gamma(m+1-p)\Gamma(n+1-q)\Gamma(l+1-m)}+ \tag{39}$$

$$\sum_{i=0}^{\infty}\sum_{j=0}^{\infty}\sum_{h=0}^{\infty}\sum_{l=0}^{\infty}\sum_{m=0}^{\infty}\sum_{n}^{\infty}\sum_{p}^{\infty}\sum_{q=0}^{\infty}\frac{(-1)^{l+n}(-2\psi)^i(Pr)^{1+l+\frac{i}{2}}(\delta)^{\frac{i}{2}-j+l-m}Ec\times\lambda^{\frac{i}{2}+l+1}(\hbar_1(\gamma))^{p+q+h}}{4^{1+l}\times h!i!j!p!q!m!n!\times(K+Ha^2)^{-\frac{i}{2}+j+l+n}\times\hbar_0(\gamma))^{h-j-\gamma m-n+q+p}\times\mathcal{S}^{2+h-\gamma j-\gamma n-\gamma m+p+q}}\times$$

$$\frac{\Gamma\left(\frac{i}{2}+1\right).\Gamma(j+l)\Gamma(l+1).\Gamma(q+l)\Gamma(m+1)\Gamma(n+l)}{\Gamma(1-j+i).\Gamma(j+1-h)\Gamma(l)\Gamma(m+1-p)\Gamma(n+1-q)\Gamma(l+1-m)}$$

Using inverse Laplace transforms in Eq. (38), leads to:

$$\mathcal{T}(\psi,t)=t+\sum_{i=1}^{\infty}\sum_{j=0}^{\infty}\sum_{h=0}^{\infty}\frac{(-\psi)^i(Pr)^{\frac{i}{2}}\times(\delta)^{\frac{i}{2}-j}(k_1(\gamma))^h}{i!j!h!k_0(\gamma))^{h-j}.}\times\frac{t^{h-\gamma j}\Gamma\left(\frac{i}{2}+1\right)\Gamma(j+1)}{\Gamma\left(1-j+\frac{i}{2}\right)\Gamma(1+j-k)}-$$

$$\sum_{i=0}^{\infty}\sum_{j=0}^{\infty}\sum_{h=0}^{\infty}\sum_{l=0}^{\infty}\sum_{m=0}^{\infty}\sum_{n}^{\infty}\sum_{p}^{\infty}\sum_{q=0}^{\infty}\frac{(-1)^{l+n}(-\psi)^i\times Ec\times(Pr)^{1+l+\frac{i}{2}}(\delta)^{\frac{i}{2}-j+l-m}\times\lambda^{l+1}(k_1(\gamma))^{p+q+h}}{4^{1+l}\times h!i!j!p!q!m!n!\times(K+Ha^2)^{l+n}\times k_0(\gamma))^{h-j-\gamma m-n+q+p}}\times$$

$$\frac{t^{1+h-\gamma q-\gamma n-\gamma m+p+q}\Gamma\left(\frac{i}{2}+1\right).\Gamma(j+1)\Gamma(l+1).\Gamma(q+l)\Gamma(n+1)\Gamma(m+1)\Gamma(n+l)}{\Gamma(1-j+i).\Gamma(j+1-h)\Gamma(l)\Gamma(m+1-p)\Gamma(n+1-q)\Gamma(l+1-m)\Gamma(2+h-\gamma q-\gamma n-\gamma m+p+q)}+ \tag{40}$$

$$\sum_{i=0}^{\infty}\sum_{j=0}^{\infty}\sum_{h=0}^{\infty}\sum_{l=0}^{\infty}\sum_{m=0}^{\infty}\sum_{n}^{\infty}\sum_{p}^{\infty}\sum_{q=0}^{\infty}\frac{(-1)^{l+n}(-2\psi)^i\times Ec\times(Pr)^{1+l+\frac{i}{2}}(\delta)^{\frac{i}{2}-j+l-m}\times\lambda^{\frac{i}{2}+l+1}(k_1(\gamma))^{p+q+h}}{4^{1+l}\times h!i!j!p!q!m!n!\times(K+Ha^2)^{-\frac{i}{2}+j+l+n}\times k_0(\gamma))^{h-j-\gamma m-n+q+p}}\times$$

$$\frac{t^{1+h-\gamma j-\gamma n-\gamma m+p+q}\Gamma\left(\frac{i}{2}+1\right).\Gamma(j+1)\Gamma(l+1).\Gamma(q+l)\Gamma(m+1)\Gamma(n+l)}{\Gamma(1-j+i).\Gamma(j+1-h)\Gamma(l)\Gamma(m+1-p)\Gamma(n+1-q)\Gamma(l+1-m)\Gamma(2+h-\gamma j-\gamma n-\gamma m+p+q)}$$

In coating processes, heat transfer characteristics at the wall are critical. The Nusselt number can be used to compute the rate of heat transfer at the boundary (and also quantifies the relative contribution of thermal convection to thermal conduction). It is defined as:

$$\mathrm{Nu}=-\frac{\partial\mathcal{T}(\psi,t)}{\partial\psi}|_{\psi=0} \tag{41}$$

Using inverse Laplace transforms we obtain:

$$\mathrm{Nu}=-\frac{\partial}{\partial\psi}\mathcal{L}^{-1}\left\{\overline{\mathcal{T}}(\psi,\mathcal{S})\right\}|_{\psi=0} \tag{42}$$

The final result is:

$$\mathrm{Nu}=\mathcal{L}^{-1}\left\{\frac{\sqrt{\mathrm{Pr}\left[\left\{\frac{k_1(\gamma)}{\mathcal{S}}+k_0(\gamma)\right\}\mathcal{S}^{\gamma}+\delta\right]}}{\mathcal{S}}+\frac{2\lambda\mathrm{EcPr}A^{\frac{3}{2}}}{\mathcal{S}^2\left(4A+\mathrm{Pr}\left[\left\{\frac{k_1(\gamma)}{\mathcal{S}}+k_0(\gamma)\right\}\mathcal{S}^{\gamma}+\delta\right]\right)}-\frac{\lambda\mathrm{EcPr}A\sqrt{\mathrm{Pr}\left[\left\{\frac{k_1(\gamma)}{\mathcal{S}}+k_0(\gamma)\right\}\mathcal{S}^{\gamma}+\delta\right]}}{\mathcal{S}^2\left(4A+\mathrm{Pr}\left[\left\{\frac{k_1(\gamma)}{\mathcal{S}}+k_0(\gamma)\right\}\mathcal{S}^{\gamma}+\delta\right]\right)}\right\} \tag{43}$$

Results and discussions

Extensive computations have been executed in MATHCAD software to evaluate the closed-form solutions derived in Section Laplace transform solutions, for variation in all key emerging dimensionless multi-physical parameters in the model. The results are given in Tables 1, 2, and 3 for Sherwood number (Sh), Nusselt number (Nu), and skin friction (*Cf*). Graphical visualizations of the influence of key parameters, such as dimensionless time (*t*), dimensionless permeability parameter (*K*), modified Hartmann magnetic number (Ha), Casson viscoplastic parameter (ς), Prandtl number (Pr), Eckert (viscous heating) number (Ec), heat generation (source) parameter (δ), Schmidt number (Sc), Damköhler number (D_v), activation energy parameter (E_a), and fractional parameters (α, γ), on velocity, $\overline{\mathcal{U}}(\psi,\mathcal{S})$ temperature, $\overline{\mathcal{T}}(\psi,\mathcal{S})$ and species concentration $\overline{\mathcal{C}}(\psi,\mathcal{S})$ are addressed in Figs. 2–15. The parameter ranges and relevant material or transport properties were selected from values reported in the cited literature, namely Sowmiya *et al.*[12], Zahid *et al.*[5], Crank and Park[18], Espuche[19], Alwuthaynani *et al.*[26], Rehman *et al.*[30], Rehage and Kind[45] and Malik *et al.*[52], while the profiles and transport quantities presented here were calculated from the present mathematical model. The simulations are based on parameter ranges adopted from the cited literature and are intended to provide theoretical insight into Casson viscoplastic transport under the specified conditions. Some limited comparisons with previous studies neglecting porous media, magnetic field, heat generation, activation energy and viscous heating effects, have also been included.

Tables 1, 2, and 3 illustrate the influence of fractional parameter (γ) and time (*t*) on skin friction, Sherwood number, and Nusselt number, respectively. Table 1 shows that the Sherwood number (Table 1) generally increases with time, indicating an increase in the mass-transfer rate of the reactive species at the wall. Nevertheless, with increasing fractional parameter (γ) there is a suppression in Sherwood number at all times. The fractional

Table 1 – *Sherwood number against different values of α and t*

α	Sh $t = 1$	Sh $t = 1.5$	Sh $t = 2$
0.1	1.534	1.619	1.699
0.2	1.502	1.567	1.629
0.3	1.471	1.519	1.565
0.4	1.44	1.473	1.506
0.5	1.409	1.431	1.453
0.6	1.379	1.391	1.404
0.7	1.349	1.353	1.36
0.8	1.32	1.318	1.321
0.9	1.29	1.286	1.285

Table 2 – *Skin friction for different values of α and t*

α	*Cf* $t = 1$	*Cf* $t = 1.5$	*Cf* $t = 2$
0.1	1.82	1.892	1.96
0.2	1.794	1.848	1.90
0.3	1.768	1.808	1.846
0.4	1.742	1.77	1.797
0.5	1.717	1.735	1.753
0.6	1.692	1.702	1.713
0.7	1.667	1.671	1.677
0.8	1.643	1.642	1.645
0.9	1.619	1.616	1.616

Table 3 – *Nusselt number by varying values of α and t*

α	Nu $t = 1$	Nu $t = 1.5$	Nu $t = 2$
0.1	5.231	5.778	6.271
0.2	5.238	5.713	6.131
0.3	5.233	5.638	6.985
0.4	5.216	5.552	5.834
0.5	5.189	5.457	5.678
0.6	5.15	5.354	5.518
0.7	5.099	5.243	5.355
0.8	5.038	5.125	5.191
0.9	4.964	5.00	5.026

parameter (γ) describes memory effects and anomalous diffusion in heterogeneous environments. It fundamentally alters transport rates and boundary-layer behavior compared with classical models for which $\gamma = 0$. Increasing the fractional order (moving away from zero) reduces memory and non-local effects within the medium. This physically suppresses the rate of mass diffusion, leading to a more gradual buildup of concentration over time towards the boundary. Sherwood number is therefore decreased. Compared to the classical model, a thinner species boundary-layer thickness is produced. Table 2 shows that skin friction is also generally enhanced with time from $t = 1$, through 1.5 to 2, at value of fractional parameter up to 0.8. For $\gamma = 0.8$, 0.9, a fluctuating response was observed, where Sherwood number initially decreased with time elapse and then increased. Table 3 shows that Nusselt number consistently increased with time (t) at all values of fractional parameter. With an increase in fractional parameter there was a sustained reduction in Nusselt number magnitudes. Lowering the fractional parameter (γ) generally accelerated the initial decline in temperature, as well as accelerated the transition to a steady state, and suppressed heat propagation compared with classical (integer-order) models. This led to a lower bulk temperature and greater net flux of heat to the boundary, i.e., higher Nusselt number. Fractional models account for the history of the temperature gradient. A lower fractional parameter means the system "remembers" past states differently, altering how current heat flux responds to previous temperatures. At lower values of fractional parameter decreases, the amplitude of thermal waves and temperature drops faster. However, the opposite effect is induced at higher values of fractional parameter where temperatures in the bulk Casson polymer are boosted and the net heat flux to the boundary is therefore suppressed. This produces a steady decline in Nusselt numbers and a cooling effect at the boundary.

Figs. 2–5 visualize the impact of selected parameters on species concentration profiles. Fig. 2 shows that, as the values of the non-integer fractional derivative parameter (γ) increase, the concentration magnitude is suppressed. Increasing the fractional derivatives parameter improves the system's memory effects. These effects decrease mass diffusion and slow species transport. The fractional parameter alters the shape and spread of the concentration profiles by introducing non-local memory effects and anomalous diffusion. In many models (like those using Caputo or Riemann-Liouville derivatives), lowering the fractional parameter reduces the rate at which a species diffuses. This causes the concentration of the diffusing substance to be higher near the wall, while plummeting much faster in the surrounding regions compared to standard integer-order diffusion. Unlike standard Fickian diffusion, fractional derivatives consider the past history. A higher fractional parameter signifies a faster "hereditary effect," allowing the concentration profile

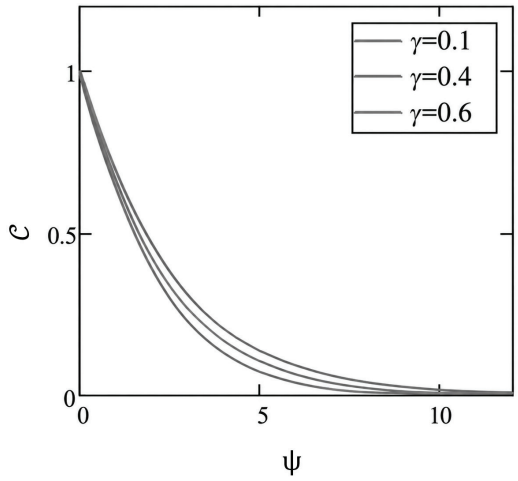


Fig. 2 – *Concentration $\overline{C}$ profiles with fractional derivative parameter, γ = 0.1, 0.4, and 0.6*

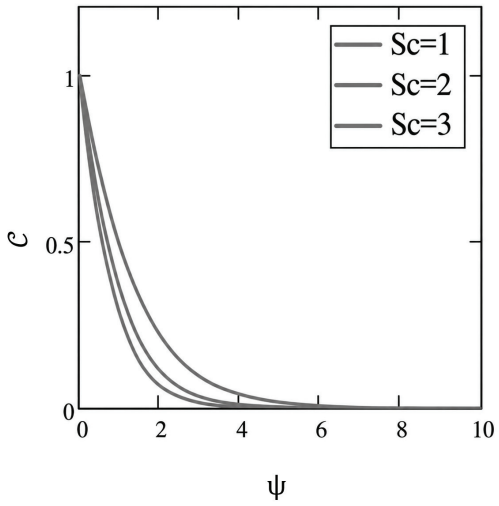


Fig. 3 – *Concentration $\overline{C}$ profiles with Schmidt number, Sc = 1, 2, and 3*

to distribute or dissipate more rapidly over time and space. Fig. 3 shows that the concentration magnitudes decrease as Schmidt number rises. A higher Schmidt number corresponds to a decrement in mass diffusivity. This inhibits molecular diffusion and produces a decrease in concentration boundary layer, resulting in a decrease in the concentration profile. The implication in coating applications is that lower molecular diffusivity species produce weakened mass diffusion and this can affect the constitution of final products including coating quality. Asymptotically smooth convergence of profiles is achieved for high values of transverse coordinate, ψ. Fig. 4 demonstrates the outcome of activation energy parameter (E_a) on concentration. It is observed that chemical reaction slows down by increasing the value of activation energy, which reduces the consumption. A low activation energy means that a larger percentage of total collisions will result in a reaction. A high activation energy restricts reactions, making the increased collision frequency from higher concentrations especially critical to drive the process forward. This is crucial in reactive polymer processing, and higher activation energy is beneficial for elevating concentration magnitudes. Fig. 5 shows that concentration profiles are markedly modified by an increase in the Damköhler number. A higher Damköhler number increases the dominance of the reaction, increasing species consumption and decreasing concentration. It expresses the rate of a chemical reaction to the rate of mass transport (such as diffusion or mixing). It determines how a reaction's speed affects the local concentration of reactants and products in a system. In the context of polymer coatings**,** the Damköhler number determines whether a coating process (or its final performance) is kinetically controlled or

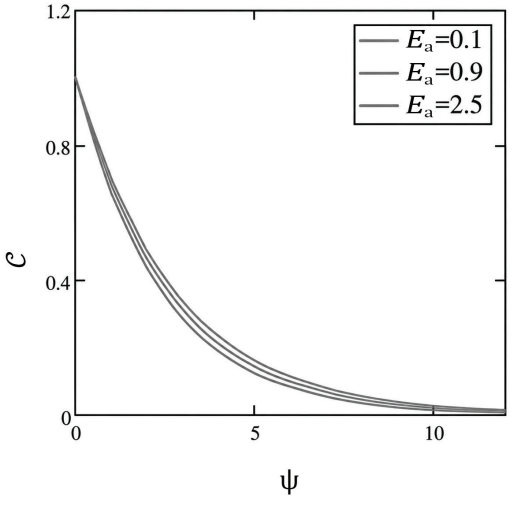


Fig. 4 – *Concentration $\overline{C}$ profiles with activation energy parameter, E_a = 0.1, 0.9, and 2.5*

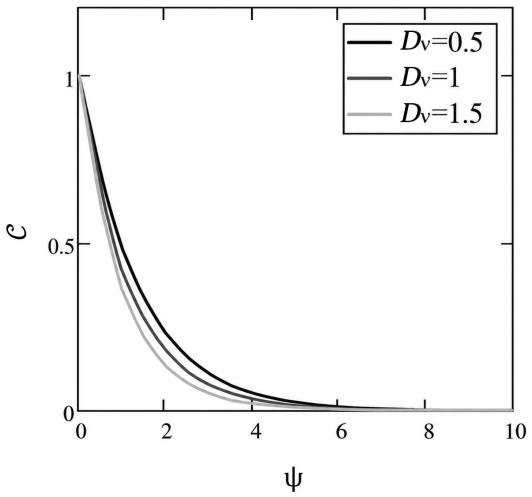


Fig. 5 – *Concentration $\overline{C}$ profiles with Damköhler number D_v = 0.5, 1, and 1.5*

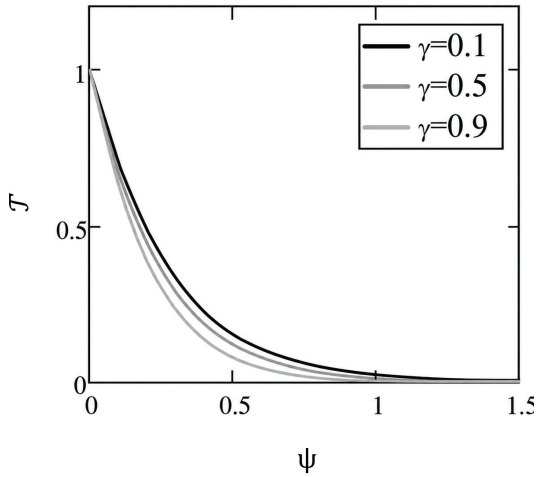


Fig. 6 – *Temperature $\overline{T}$ profiles with fractional derivative parameter γ = 0.1, 0.5, and 0.9*

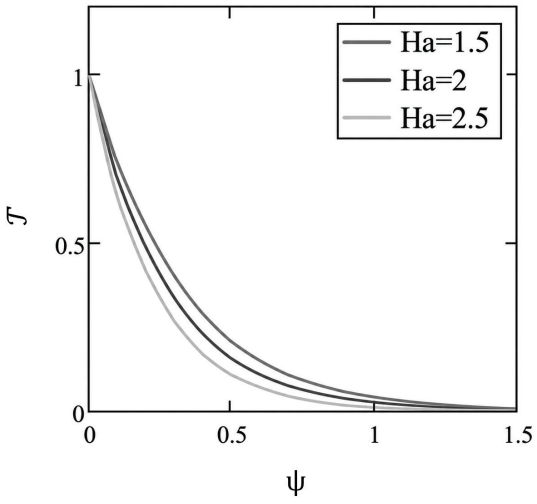


Fig. 7 – *Temperature $\overline{T}$ profiles with magnetic parameter, Ha = 1.5, 2, and 2.5*

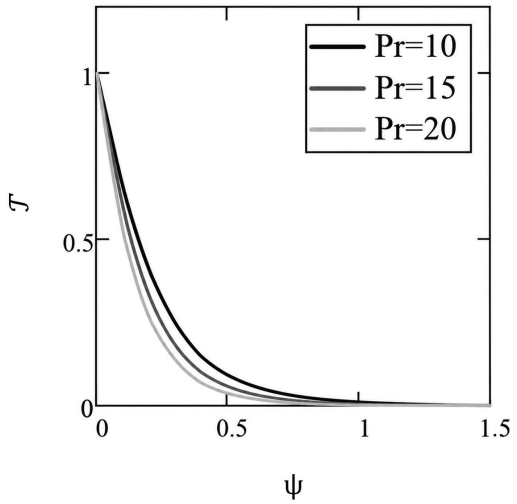


Fig. 8 – *Temperature $\overline{T}$ profiles with Prandtl number, Pr = 10, 15, and 20*

mass-transfer (diffusion) limited. For D_v <<1, the rate of mixing or diffusion is much faster than the chemical reaction. Therefore, reactants are homogeneously dispersed throughout the system before they can significantly react. The concentration of reactants remains high and uniform, while the concentration of products remains very low. As D_v increases to 0.5, which is a moderate value, the time required for the reaction becomes comparable to the time required for mixing or mass transport. This produces substantial concentration gradients within the system. When D_v = 1, the rate of a chemical reaction becomes equal to the rate of mass transport (convective diffusion or mixing) and there is a reduction in concentration magnitudes, as observed in the graph. With further increment in D_v, the speed of the chemical reaction is elevated, and concentration magnitudes are further suppressed. We do not consider the extreme case, D_v >> 1, for which chemical reaction occurs incredibly fast compared to how quickly reactants can mix or diffuse into the system. In this case, the reaction consumes reactants instantly upon contact. The concentration of reactants drops effectively to zero at the reaction zone, and product concentration reaches its maximum potential limit. This is not recommended in polymer processing. Intermediate values of Damköhler number are more amenable to efficient polymer coating systems.

Figs. 6 – 10 display the evolution in temperature profiles with various parameters. Fig. 6 shows how the temperature graph drops as the values of the non-integer fractional order derivative parameter rise. Stronger thermal memory effects cause the temperature distribution to decrease and heat diffusion to be suppressed as the value of the fractional derivative parameter increases. Fig. 7 explains the relationship between Hartmann magnetic number and the temperature distribution, $\overline{T}$. As the Hartmann number rises, the Casson fluid temperature declines. While this is not observed in conventional Newtonian flows, it can arise in magnetic polymers. The Lorentz force decelerates the polymer near the boundary, suppressing natural convection. In the present formulation, increasing the magnetic parameter modifies the velocity field through Lorentz-force dampening and consequently alters convective heat transport, producing the temperature trend observed in the numerical solution. This produces a decrement in thermal boundary-layer thickness.

Fig. 8 illustrates that the temperature drops as the Prandtl number (Pr) increases. The Prandtl number is defined as the relation of momentum diffusivity to thermal diffusivity. When dynamic viscosity and specific heat capacity are kept constant, (Pr) is inversely proportional to thermal conductivity. A

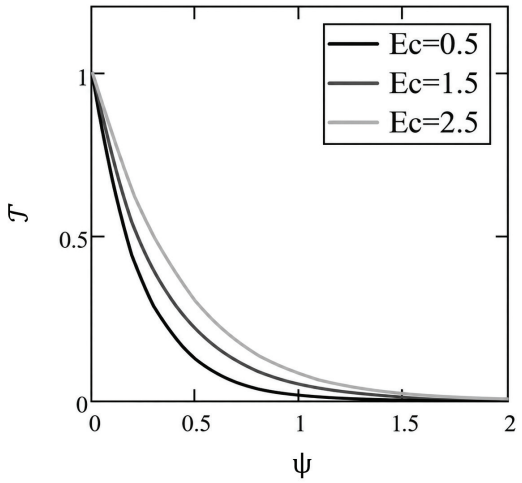


Fig. 9 – *Temperature $\overline{\mathcal{T}}$ profiles with Eckert number, Ec = 0.5, 1.5, and 2.5*

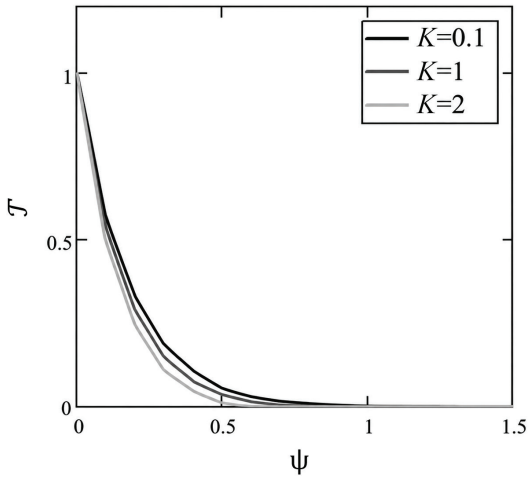


Fig. 10 – *Temperature $\overline{\mathcal{T}}$ profiles with permeability parameter, K = 0.1, 1, and 2*

higher Prandtl number is encountered in polymers, and they possess lower thermal diffusivity, resulting in a steeper temperature gradient. Thermal diffusion is depleted and this decreases temperatures, with this trend being sustained at all locations transverse to the wall. Thermal boundary-layer thickness is also reduced.

Fig. 9 shows the influence of Eckert number (Ec) on the temperature distribution. As the Eckert number increases, the temperature profile noticeably rises. Stronger frictional heating in the polymer is produced with greater viscous dissipation, which converts mechanical energy into thermal energy. The intermolecular collisions and frictional heating (viscous dissipation) release energy, which acts as an internal heat source, warming the fluid. This energizes the polymer and elevates temperatures. The inclusion of viscous heating in polymer coating models is therefore recommended and produces more realistic estimates of temperature characteristics.

Fig. 10 illustrates the effect of the permeability parameter (K) on temperature. As permeability increases, the percentage concentration of solid matrix fibers in the porous medium is reduced. The polymer can flow more easily through a higher permeability medium than a lower one as the Darcian drag force is diminished. This accelerates the flow but suppresses thermal conduction between solid particles around the pores, manifesting in a reduction in temperature. Higher permeability therefore produces a cooling effect whereas lower permeability produces a heating effect, both of which may be exploited in thermal management of polymer coating processes.

Fig. 11 illustrates the impact of heat generation ($\delta < 0$) / generation ($\delta > 0$) on temperature. The temperature field increases significantly when the heat generation parameter rises. The fluid's thermal energy is increased and the local temperature is raised by the thermal energy generated within the system. The fluid receives more thermal energy at a higher rate of heat generation, which enhances the diffusion of heat from the wall into the surrounding fluid and causes the thermal boundary layer to thicken. This behavior is consistent with the current energy equation's positive heat-generation term.

Figs. 12–15 illustrate the evolution in velocity profiles $\overline{\mathcal{U}}$ with various parameters. Fig. 12 shows that, with an increase in fractional derivative parameter γ, the velocity decreases. The polymer motion is delayed and there is an escalation in memory effect. This decelerates the flow and increases momentum (hydrodynamic) boundary-layer thickness. Fractional calculus enables engineers to define the memory and non-local hereditary effects of polymer chains. In viscoplastic polymers, the fractional parameter controls the material's memory, relaxation

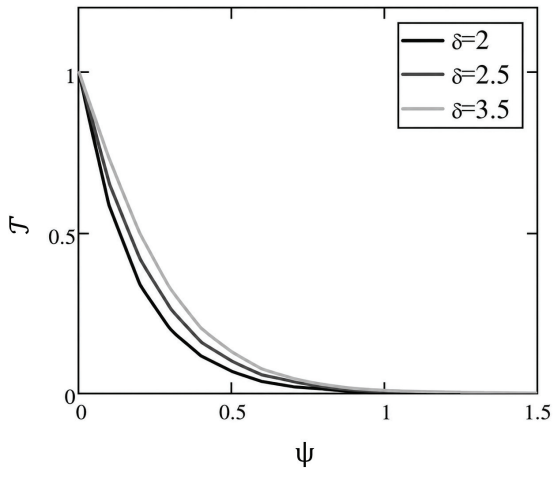


Fig. 11 – *Temperature $\overline{\mathcal{T}}$ profiles with heat generation (source) parameter, δ = 2, 2.5, and 3.5*

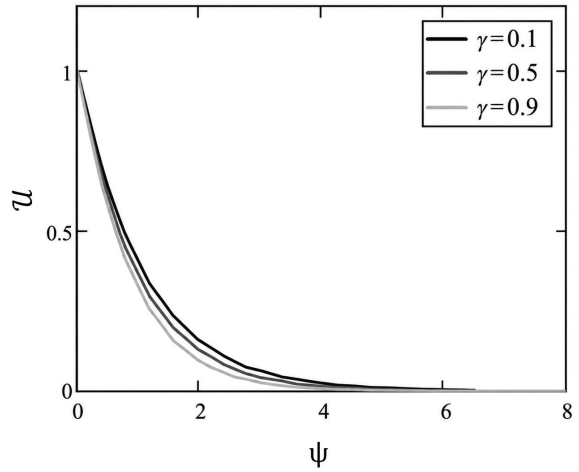


Fig. 12 – *Velocity $\overline{u}$ profiles with fractional derivative parameter γ = 0.1, 0.5, and 0.9*

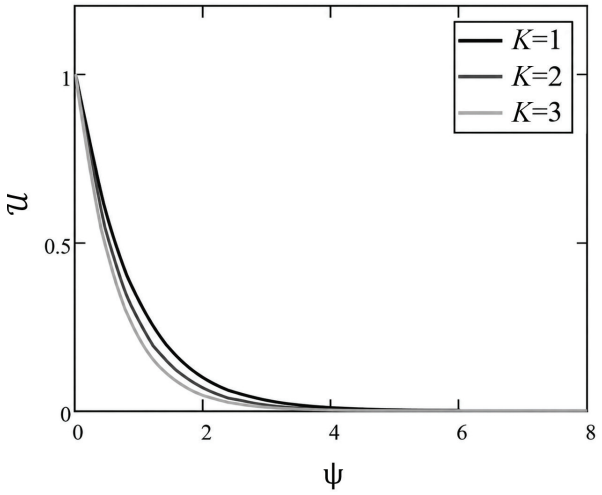


Fig. 13 – *Velocity $\overline{u}$ profiles with permeability parameter, K = 1, 2, and 3*

spectrum, and transition between solid-like elastic and liquid-like viscous behaviors. Adjusting this parameter directly dictates how fast the polymer flows and yields under stress. The inclusion of fractional effects therefore provides the coating engineer with a greater range of sensitivity with which to assess viscoplastic behavior, in particular momentum diffusion which influences velocity characteristics. Compared with the classical Casson formulation, the present fractional extension introduces an additional parameter for representing non-local temporal memory effects.

Fig. 13 shows that, with greater permeability, *K,* the velocity is suppressed. Greater permeability can reduce polymer velocities in porous media, even though the Darcian impedance is also reduced with higher permeability. This counter-intuitive behavior occurs when permeability increases, the fluid is spread across a wider total volume and faces less flow resistance, meaning the superficial (Darcy) velocity drops relative to the injection rate in polymer coating flows. While for Newtonian fluids, Darcy's law asserts that flow rate and velocity increase linearly with permeability, for viscoplastic polymer solutions, the relationship is nonlinear due to their complex rheology. As polymers squeeze through interconnected porous matrices, they experience transient stretching in pore-throat constrictions. If the pore geometry allows a higher flow rate, the polymer chains may stretch drastically. The observed permeability dependence should be attributed to the terms explicitly retained in the present Casson–Darcy formulation; polymer-chain stretching, extensional thickening and adsorption should not be invoked unless they are incorporated into the constitutive or porous-medium model. The extra flow

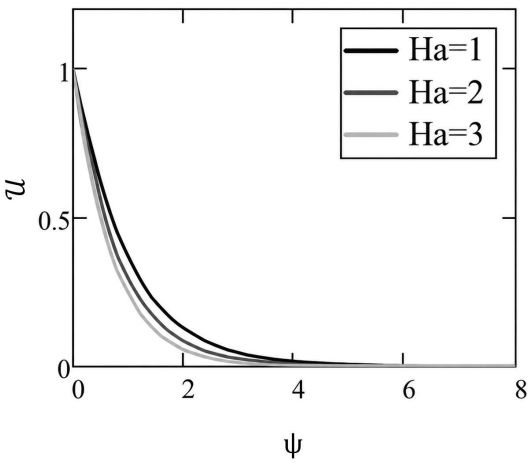


Fig. 14 – *Velocity $\overline{u}$ profiles with magnetic parameter, Ha = 1, 2, and 3*

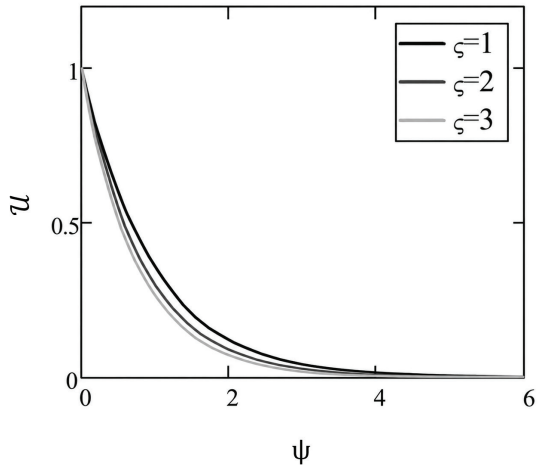


Fig. 15 – *Velocity $\overline{u}$ profiles with Casson viscoplastic parameter ς = 1, 2, and 3*

resistance created by this elasticity counters the permeability increase, effectively capping or even reducing the overall velocity. This effect has been reported in other studies, e.g., Murad *et al.*[56] Casson polymers are viscoplastic fluids and require a minimum pressure gradient (yield stress) to start flowing. In very low permeability porous media, flow can become stagnant. When permeability increases, pressure drops may redistribute across the network, reducing the driving force locally in certain paths and slowing the fluid down. A more permeable medium therefore does not always guarantee faster flow since polymers naturally adhere to pore walls. In higher permeability porous foams, as used in some coating processes, larger pore spaces allow more complex polymer conformations, promoting greater polymer adsorption and mechanical retention (plugging), which dramatically restricts flow velocity.

Fig. 14 shows the impact of Hartmann magnetic number on velocity profiles. This parameter arises in the Lorentz body force term, $-(\mathrm{Ha}^2)\mathcal{U}(\psi,t)$ in the reduced momentum Eq. (8). Increasing the Hartmann number strengthens the Lorentz-force contribution, which opposes the flow and consequently reduces the velocity magnitude. This results in a sustained depletion in velocity. External magnetic fields therefore offer a robust and non-intrusive mechanism for flow regulation in polymers.

Fig. 15 illustrates the response in velocity to Casson viscoplastic parameter (ς). This parameter features in the term, $\lambda\dfrac{\partial^2\mathcal{U}(\psi,t)}{\partial\psi^2}$ which is an augmented shear term, wherein $\lambda = 1+\dfrac{1}{s}$. The physical interpretation of increasing the Casson parameter should be stated from its mathematical definition in Eq. (8), including whether it represents an increase or decrease in the relative importance of yield stress. An upsurge in viscous resistance is therefore produced, and this inhibits momentum diffusion which leads to a suppression of the velocity field**.** The polymer becomes "thicker" and moves slower. Physically, a high Casson fluid value causes the fluid to approach less viscous and more solid-like, which induces strong flow retardation. For the case, ς = 1, Newtonian fluid behavior is retrieved.

Figs. 16–18 provide limiting-case comparisons with the results of Sene[51] after the corresponding additional physical effects are removed; these comparisons support consistency with the earlier model but do not by themselves validate the complete fractional formulation. In Fig. 16, velocity $\overline{\mathcal{U}}$ profiles are given with (K>0) and without porous media (K = 0) and with (Ha >0) and without magnetic field (Ha = 0) effects; excellent agreement is ob-

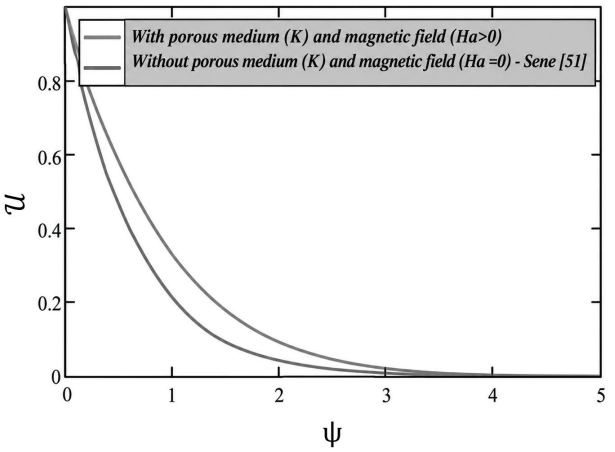


Fig. 16 – *Velocity $\overline{\mathcal{U}}$ profiles with and without porous media and magnetic field effects; comparison with Sene*[51]

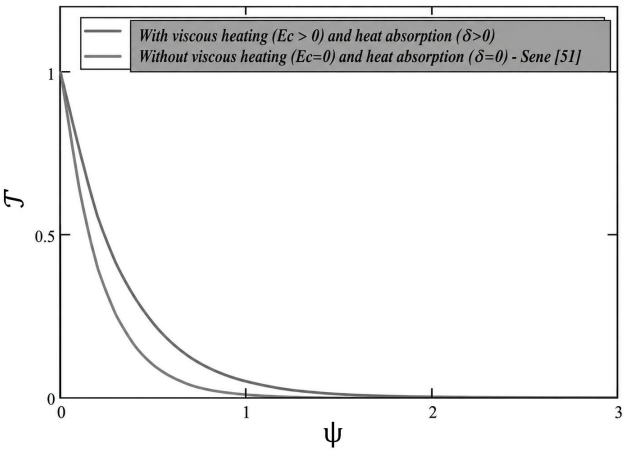


Fig. 17 – *Temperature $\overline{\mathcal{T}}$ profiles with and without viscous dissipation and heat generation effects; comparison with Sene*[51]

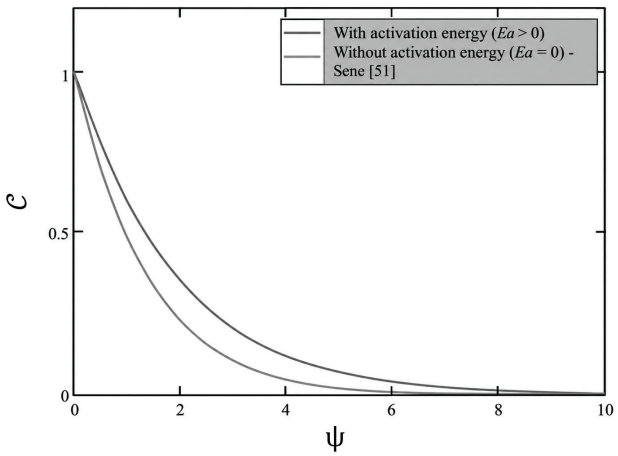


Fig. 18 – *Species concentration $\overline{\mathcal{C}}$ profiles with and without activation energy effects; comparison with Sene*[51]

tained at all values of the transverse coordinate, ψ. Fig. 17 provides a comparison of temperature $\overline{\mathcal{T}}$ profiles with (Ec > 0) and without viscous dissipation (Ec = 0) and with heat generation ($\delta > 0$) and without heat generation ($\delta = 0$) effects; again, very good correlation is achieved with Sene[51]. Finally, Fig. 18 depicts species concentration $\overline{\mathcal{C}}$ profiles with ($E_a > 0$) and without activation energy ($E_a = 0$) effects; close agreement is attained with the previous studies of Sene[51].

Conclusion

Motivated by the simulation of reactive polymer-coating processes, a mathematical model has been developed for fractional magnetohydrodynamic (MHD) polymeric Casson flow, including heat and mass transfer along a wall adjacent to a porous medium, with viscous dissipation, heat generation and activation-energy effects. Fractional derivatives have been incorporated to extend the Casson viscoplastic model, (which features shear-thinning and yield stress effects), to represent complex non-Newtonian responses and memory-dependent behavior. The mathematical formulation has been developed with the constant-proportional Caputo fractional derivative (CPCFD). The transformed, dimensionless fractional governing equations for mass, momentum, energy and species concentration were solved using the Laplace integral transform technique (LITT), under physically realistic boundary conditions. MATHCAD software was used to evaluate solutions for non-dimensional velocity, $\mathcal{U}$, temperature, $\mathcal{T}$, and concentration, C, with variation in transverse coordinate ψ and time t. Nusselt number, Sherwood number, and skin friction solutions were also tabulated for various emerging parameters. Verification with previous studies neglecting porous media, magnetic field, heat generation, activation energy and viscous heating effects was conducted. The present analytical study has shown that the following:

(i) Skin friction, Nusselt number, and Sherwood number are reduced with increasing fractional parameter (γ) but generally boosted with time (t).

(ii) An increase in activation energy parameter (E_a), i.e., minimum energy threshold required for a chemical reaction to occur, depletes the magnitude of species concentration.

(iii) A higher Damköhler number, (D_v), increases the dominance of the reaction, increasing species consumption and decreasing concentration.

(iv) An increase in fractional derivative parameter (γ) improves the system memory effects, suppresses species diffusion, and reduces concentration magnitudes.

(v) A higher Schmidt number (Sc) depletes species diffusion and concentration boundary-layer thickness.

(vi) Increasing Eckert number (Ec, viscous heating parameter) enhances temperature magnitudes, whereas higher permeability parameter reduces them.

(vii) Higher values of Casson rheological (viscoelastic yield stress) parameter (ς) decelerate the flow and increase momentum boundary-layer thickness.

(viii) An increase in magnetic parameter (Ha), i.e., stronger magnetic field intensity and Lorentzian magnetohydrodynamic drag strongly dampens the flow.

(ix) Temperature is significantly increased with higher heat generation parameter (δ).

(x) With higher permeability parameter, K, the velocity is suppressed.

The findings may be contribute to the development of more sophisticated simulations of industrial viscoplastic functional coating systems.

Limitation and future work

The present study employs a relatively simple rheological model for polymers and assumes classical Fourier heat conduction. Future work could investigate Herschel-Bulkley non-Newtonian models in addition to nanoparticle doping[57] and non-Fourier thermal relaxation effects[58]. Additionally, non-Darcy effects for polymer coatings[59] could also be explored. Despite its mathematical contributions, this study has some limitations. It employs a simplified albeit fractional viscoplastic model, invokes many geometric approximations, represents chemical reactions in a simplified manner and considers a reduced dimensionality of the model. Furthermore, the model has not been extensively validated against experimental data. Future investigations could incorporate experimental data and artificial intelligence techniques to support the optimization of industrial thermal polymer-processing applications, although this would require computational fluid dynamics (CFD) solvers and machine-learning coupling.

Nomenclature

ρ – Density of Casson polymer, kg m^{-3}
ϕ – Porous medium porosity, –
ς – Casson fluid parameter, –
υ – Kinematic viscosity of Casson polymer, m^2 s^{-1}
g – Gravitational acceleration, m^2 s^{-2}
k – Thermal conductivity, W m^{-1} K^{-1}
k_1 – Permeability of the porous medium, m^2
γ – Fractional derivative parameter, –
C_p – Specific heat constant, J kg^{-1} K^{-1}
Q_0 – Heat generation, kg m^{-1} s^{-3} K^{-1}
δ – Dimensionless heat generation parameter, –
t – Dimensionless time, –
$\mathcal{U}$ – Dimensionless velocity, –
C – Dimensionless concentration, –
k_0 – First-order reaction rate constant, s^{-1}
R – Universal gas constant, J mol^{-1} K^{-1}
σ – Electrical conductivity, S m^{-1}
Φ – Viscous dissipation, W m^{-3}
μ – Dynamic viscosity, kg m^{-1} s^{-1}
B_0 – Strength of magnetic field, **T**
Sc – Schmidt number, –
Ha – Hartmann (magnetic) number, –
Pr – Prandtl number, –
E_a – Activation energy, J mol^{-1}
Ec – Eckert number, –
D_v – Damköhler number, –
α – Fractional parameter, –
Ψ – Dimensionless transverse coordinate, –
$\mathcal{T}$ – Dimensionless temperature, –
$\mathcal{L}\{\ \}$ – Laplace transform, –
E – Dimensionless activation energy parameter, –

Abbreviations

CPC – Constant-Proportional Caputo
CPCFC – Constant-Proportional Caputo Fractional Derivative
LITT – Laplace Integral Transformation Technique
MHD – Magnetohydrodynamic

References

1. *Yadav, D., Awasthi, M. K., Al-Azri, H. M.* (Eds.), Non-Newtonian Fluids for Industrial Applications: Modeling and Simulations, Wiley, USA, 2026. doi: https://doi.org/10.1002/9781394356256
2. *Sofou, S., Mitsoulis, E.*, Roll-over-web coating of pseudoplastic and viscoplastic sheets using the lubrication approximation, J. Plast. Film Sheeting, **21** (2005) 307. doi: https://doi.org/10.1177/8756087905059963
3. *Roy, A. K., Debnath, S., Bég, O. A.*, Transient solute dispersion in electro-osmotic viscoplastic flow in a microchannel, Z. Angew. Math. Mech. **103** (2023) e202200260. doi: https://doi.org/10.1002/zamm.202200260
4. *Sofou, S., Mitsoulis, E.*, Roll-over-web coating of pseudoplastic and viscoplastic sheets using the lubrication approximation, J. Plast. Film Sheeting **21** (2005) 307. doi: https://doi.org/10.1177/8756087905059963
5. *Zahid, M., Siddique, I., Ali, R.*, Coating of a viscoplastic material onto a moving porous web during forward roll coating process: A theoretical study, J. Plast. Film Sheeting **39** (2023) 19. doi: https://doi.org/10.1177/87560879221113638
6. *Islam, M. R., Hossain, A., Biswas, R., Hasan, M., Rana, B. M. J., Habibullah, Afikuzzaman, M.*, Modelling and theoretical overview of Casson fluid flow through a stretching sheet with variable viscosity and sinusoidal boundary conditions, Int. J. Ambient Energy **46** (2025) 2539139. doi: https://doi.org/10.1080/01430750.2025.2539139
7. *Kumar, V. V., Shekar, M. N. R., Bejawada, S. G.*, Thermo-diffusion, diffusion-thermo impacts on heat and mass transfer Casson fluid flow with porous medium in the presence of heat generation and radiation, Partial Differ. Equ. Appl. Math. **13** (2025) 101039. doi: https://doi.org/10.1016/j.padiff.2024.101039
8. *Shahidi, A., Wei, W., Bhatti, M. M., Bég, O. A., Bég, T. A.*, Mixed convection Casson polymeric flow from a nonlinear stretching surface with radiative flux and non-Fourier thermal relaxation effects: Computation with CSNIS, Z. Angew. Math. Mech. **103** (2023) e202200519. doi: https://doi.org/10.1002/zamm.202200519
9. *Castro, D. J., Song, J. O., Lade, R. K., Francis, L. F.*, Magnetic microrheology for characterization of viscosity in coatings, in: Wen, M., Dušek, K. (Eds.), Protective Coatings, Springer, Cham, 2017. doi: https://doi.org/10.1007/978-3-319-51627-1_5
10. *Boz, E. B., Bondre, A., de Bruijne, R., Forner-Cuenca, A.*, Conductive polymer coatings control reaction selectivity in all-iron redox flow batteries, Adv. Mater. **37** (2025) e2414596. doi: https://doi.org/10.1002/adma.202570174
11. *Kausar, M. S., Bég, O. A., Waqas, M., Zamri, N., Khan, M. I.*, Analytical computations for thermally radiative couple-stress viscoplastic magnetized nanomaterial capturing gyrotactic microorganisms, non-Darcian and transpiration aspects: A model for enhanced heat transference in modern industrial processes, Fuel **377** (2024) 132564. doi: https://doi.org/10.1016/j.fuel.2024.132564
12. *Sowmiya, C., Kumar, B. R., Bég, O. A., Kuharat, S.*, Modeling and analysis of MHD free convective thermo-solutal transport in Casson fluid flow with radiative heat flux, J. Therm. Anal. Calorim. **149** (2024) 6195. doi: https://doi.org/10.1007/s10973-024-13115-6
13. *Vasu, B., Ray, A. K., Bég, O. A., Gorla, R. S. R.*, Magneto-bioconvection flow of a Casson thin film with nanoparticles over an unsteady stretching sheet: HAM and GDQ computation, Int. J. Numer. Methods Heat Fluid Flow **29** (2019) 4277. doi: https://doi.org/10.1108/hff-02-2019-0158
14. *Nasir, M., Kausar, M. S., Waqas, M., Bég, O. A., Abdullaev, S. S., Saadaoui, S., Khan, W. A.*, Computational analysis of magnetized Casson liquid stretching flow adjacent to a porous medium with Joule heating, stratification, multiple slip and chemical reaction aspects, Numer. Heat Transf. A Appl. **86** (20245) 4464. doi: https://doi.org/10.1080/10407782.2024.2319722

15. *Sreenivasulu, P., Poornima, T., Ragavi, M., Vinothkumar, B., Rao, A. S., Bég, O. A., Bég, T. A.*, Computation of Casson non-Newtonian thermo-magnetic SWCNT/MWCNT-based hybrid nanofluid coating flow from a cylinder with multiple slip and radiative flux effects, Int. J. Comput. Mater. Sci. Eng. **14** (2025) 2550018. doi: https://doi.org/10.1142/s2047684125500186
16. *Friedrich, J. F., Unger, W. E. S., Lippitz, A., Koprinarov, I., Kühn, G., Weidner, S., Vogel, L.*, Chemical reactions at polymer surfaces interacting with a gas plasma or with metal atoms—their relevance to adhesion, Surf. Coat. Technol. **116–119** (1999) 772. doi: https://doi.org/10.1016/s0257-8972(99)00229-7
17. *Gilliam, M.*, Polymer surface treatment and coating technologies, in: Nee, A. (Ed.), Handbook of Manufacturing Engineering and Technology, Springer, London, 2013, pp. 99–124. doi: https://doi.org/10.1007/978-1-4471-4670-4_20
18. *Crank, J., Park, G. S.* (Eds.), Diffusion in Polymers, Academic Press, New York, 1968.
19. *Espuche, E.*, in: Boudenne, A., Candau, Y., Ibos, L., Sabu, T. (Eds.), Handbook of Multiphase Polymer Systems, 1st ed., John Wiley & Sons, Chichester, UK, 2011, pp. 749–770. doi: https://doi.org/10.1002/9781119972020.ch19
20. *Bhatti, M. M., Michaelides, E. E.*, Study of Arrhenius activation energy on the thermo-bioconvection nanofluid flow over a Riga plate, J. Therm. Anal. Calorim. **143** (2021) 2029. doi: https://doi.org/10.1007/s10973-020-09492-3
21. *Reddy, B. S., Goud, B. S.*, Transportation of MHD Casson fluid with dissipation, radiation impact under Dufour effect over an exponentially stretching surface with activation energy: A numerical study, Model. Earth Syst. Environ. **12** (2026) 28. doi: https://doi.org/10.1007/s40808-025-02677-5
22. *Aarathi, T., Anala, S. R., Jagadeshkumar, K., Prasad, V. R., Bég, O. A.*, Entropy generation in a chemically reactive MHD unsteady micropolar nanofluid flow with activation energy over an inclined stretching sheet: A Buongiorno model approach, Proc. Inst. Mech. Eng. Part E J. Process Mech. Eng. **240** (2026) 2044. doi: https://doi.org/10.1177/09544089241272900
23. *Prabu, D., Abbas, S., Inam, I., Bayram, M., Abdullaeva, B., Al Agha, A., Al Garalleh, H., Mahariq, I.,* Cattaneo–Christov model for Marangoni convection in Casson fluid with thermal radiation and activation energy under dual-phase heat transfer, Int. J. Thermofluids **30** (2025) 101413. doi: https://doi.org/10.1016/j.ijft.2025.101413
24. *Zhang, L., Bhatti, M. M., Shahid, A., Ellahi, R., Bég, O. A., Sait, S. M.*, Nonlinear nanofluid flow under the consequences of Lorentz forces and Arrhenius kinetics through a permeable surface: A robust spectral approach, J. Taiwan Inst. Chem. Eng. **124** (2021) 98. doi: https://doi.org/10.1016/j.jtice.2021.04.065
25. *Nadeem, S., Hafeez, K., Alzabut, J., Zidan, A. M., Zigta, B.*, Unsteady two-dimensional flow of non-Newtonian fractional Casson fluid for an edge with heated boundaries, Sci. Rep. **15** (2025) 38532. doi: https://doi.org/10.1038/s41598-025-20493-w
26. *Alwuthaynani, M., Ishtiaq, U., Khalifa, H. A. E.-W., Alburaikan, A., Idress, R., Popa, I. L.*, Fractional-order modelling and analytical solutions for MHD Casson fluid flow in an inclined channel with heat and mass transfer, Sci. Rep. **15** (2025) 39790. doi: https://doi.org/10.1038/s41598-025-23478-x
27. *Srivastava, V., Tripathi, D., Srivastava, P. K., Kuharat, S., Bég, O. A.*, Mathematical modelling of oxygen diffusion from capillary to tissues during hypoxia through multiple points using fractional balance equations with memory, Crit. Rev. Biomed. Eng. **52** (2024) 1. doi:https://doi.org/10.1615/CritRevBiomedEng.2024053461
28. *Channakote, M. M., Bég, O. A., Kuharat, S., Shekar, M., Siddabasappa, C.*, Electro-osmotically modulated visco-elastic SWCNT-blood flow in symmetric/non-symmetric stenosed arteries with heat generation using a fractional second-grade model, Int. J. Comput. Mater. Sci. Eng. **14** (2025) 2550026. doi: https://doi.org/10.1142/S2047684125500265
29. *Tripathi, D., Bég, O. A.*, Mathematica numerical simulation of peristaltic biophysical transport of a fractional viscoelastic fluid through an inclined cylindrical tube, Comput. Methods Biomech. Biomed. Eng. **18** (2014) 1648. doi: https://doi.org/10.1080/10255842.2014.940332
30. *Rehman, A. U., Riaz, M., Khan, I., Mohamed, A.*, Time fractional analysis of Casson fluid with application of novel hybrid fractional derivative operator, AIMS Math. **8** (2023) 8185. doi: https://doi.org/10.3934/math.2023414
31. *Ahmad, A., Nazar, M., Ahmad, M., Eldin, S. M., Nisa, Z. U., Waqas, H., Imran, M.*, Application of constant proportional Caputo fractional derivative to thermodiffusion flow of MHD radiative Maxwell fluid under slip effect over a moving flat surface with heat and mass diffusion, Adv. Math. Phys. **2024** (2024) 9306915. doi: https://doi.org/10.1155/2024/9306915
32. *Ali, F., Shah, Z., Sheikh, N. A., Alshehery, S., Khan, I., Koh, W. S.*, Bioconvection in polar fluid with microstructure: A fractional heat and mass transfer model with non-singular and non-local kernel, Results Phys. **74** (2025) 108292. doi: https://doi.org/10.1016/j.rinp.2025.108292
33. *Jamil, D. F., Uddin, S., Kazi, M., Roslan, R., Gorji, M. R., Akhir, M. K. M.*, MHD blood flow effects of Casson fluid with Caputo–Fabrizio fractional derivatives through inclined blood vessels with thermal radiation, Heliyon **9** (2023) e21780. doi: https://doi.org/10.1016/j.heliyon.2023.e21780
34. *Tabi, C. B., Ndjawa Yomi, P. A., Motsumi, T., Kamdem, C., Kofane, T. C.*, Magnetic field effect on a fractionalized blood flow model in the presence of magnetic particles and thermal radiations, Chaos Solit. Fractals **131** (2019) 109540. doi: https://doi.org/10.1016/j.chaos.2019.109540
35. *Abbas, S., Inam, I., Alharthi, A. M., AL-Khasawneh, M. A. S., Az-Zo'bi, E. A., Garalleh, H. A.,* Fractional magnetohydrodynamic Casson fluid flow with thermal radiation and buoyancy effects: A constant proportional Caputo model, Bound. Value Probl. **2025** (2025) 44. doi: https://doi.org/10.1186/s13661-025-02036-4
36. *Madhavi, K., Prasad, V. R., Gaffar, S. A.*, Darcy flow of polymer from an inclined plane with convective heat transfer analysis: A numerical study, J. Therm. Anal. Calorim. **146** (2021) 117. doi: https://doi.org/10.1007/s10973-020-09942-y
37. *Chauveteau, G.*, Fundamental criteria in polymer flow through porous media, in: Water-Soluble Polymers, Advances in Chemistry, American Chemical Society, Washington, DC, 1986, pp. 227-267. doi: https://doi.org/10.1021/ba-1986-0213.ch014
38. *Chen, H., Poitzsch, M. E.*, Dynamics of polymers flowing through porous media: Interplay of solvent properties, flow rates and wetting, Macromolecules **55** (2022) 11068. doi: https://doi.org/10.1021/acs.macromol.2c01902

39. *Bég, O. A., Makinde, O. D.*, Viscoelastic flow and species transfer in a Darcian high-permeability channel, J. Pet. Sci. Eng. **76** (2011) 93. doi: https://doi.org/10.1016/j.petrol.2011.01.008
40. *Lawal, A., Kalyon, D. M.*, Viscous heating in non-isothermal die flows of viscoplastic fluids with wall slip, Chem. Eng. Sci. **52** (1997) 1323. doi: https://doi.org/10.1016/S0009-2509(96)00486-1
41. *Winter, H. H.*, Viscous dissipation in shear flows of molten polymers, in: Advances in Heat Transfer, in: Hartnett, J. P., Irvine, T. F. (Eds.), Vol. 13, Elsevier, 1977, pp. 205–267. doi: https://doi.org/10.1016/S0065-2717(08)70224-7
42. *Wang, F. Z., Animasaun, I. L., Shah, N. A., Muhammad, T.*, Thermo-solutocapillarity boundary layer flow: Insight into adsorption and desorption surface kinetics, Int. Commun. Heat Mass Transf. **178** (2026) 111612. doi: https://doi.org/10.1016/j.icheatmasstransfer.2026.111612
43. *Animasaun, I. L., Muhammad, T., Yook, S.-J.*, Exploration of half-cycle length of converging circular wavy duct with diverging-outlet: Turbulent water dynamics, Adv. Theory Simul. **8** (2025) 2500038. doi: https://doi.org/10.1002/adts.202500038
44. *Wang, F., Animasaun, I. L., Muhammad, T.*, Anisotropic turbulent flow of water through converging wavy-aluminum-circular pipe with five half-cycles: Insight into the significance of four-branch minor-inlet angle, J. Non-Equilib. Thermodyn. **50** (2025) 513. doi: https://doi.org/10.1515/jnet-2025-0046
45. *Rehage, H., Kind, M.*, The first Damköhler number and its importance for characterizing the influence of mixing on competitive chemical reactions, Chem. Eng. Sci. **229** (2021) 116007. doi: https://doi.org/10.1016/j.ces.2020.116007
46. *Ge, J., Peters, B.*, Mass transfer in catalytic depolymerization: External effectiveness factors and serendipitous processivity in stagnant and stirred melts, Chem. Eng. J. **466** (2023) 143251. doi: https://doi.org/10.1016/j.cej.2023.143251
47. *Roy, A. K., Bég, O. A., Shaw, S., Mashiku, L. R., Bég, T. A.*, Solute dispersion in a permeable capillary with wall exchange: Darcy flow model, Korea-Aust. Rheol. J. **37** (2025) 1. doi: https://doi.org/10.1007/s13367-024-00116-y
48. *Abbas, I., Hobiny, A., Alshehri, H., Vlase, S., Marin, M.*, Analysis of thermoelastic interaction in a polymeric orthotropic medium using the finite element method, Polymers **14** (2022) 2112. doi: https://doi.org/10.3390/polym14102112
49. *Gaffar, S. A., Prasad, V. R., Bég, O. A., Khan, M. H. H., Venkatadri, K.*, Radiative and magnetohydrodynamics flow of third-grade viscoelastic fluid past an isothermal inverted cone in the presence of heat generation/absorption, J. Braz. Soc. Mech. Sci. Eng. **40** (2018) 127. doi: https://doi.org/10.1007/s40430-018-1049-0
50. *Kumar, V. V., Shekar, M. N. R., Bejawada, S. G.*, Thermo-diffusion, diffusion-thermo impacts on heat and mass transfer Casson fluid flow with porous medium in the presence of heat generation and radiation, Partial Differ. Equ. Appl. Math. **13** (2025) 101039. doi: https://doi.org/10.1016/j.padiff.2024.101039
51. *Sene, N.*, Analytical solutions of a class of fluids models with the Caputo fractional derivative, Fractal Fract. **6** (2022) 35. doi: https://doi.org/10.3390/fractalfract6010035
52. *Malik, H. T., Farooq, M., Ahmad, S., Mohamed, M. M. I.*, Convective heat transportation in exponentially stratified Casson fluid flow over an inclined sheet with viscous dissipation, Case Stud. Therm. Eng. **52** (2023) 103720. doi: https://doi.org/10.1016/j.csite.2023.103720
53. *Baleanu, D., Fernandez, A., Akgül, A.*, On a fractional operator combining proportional and classical differintegrals, Mathematics **8** (2020) 360. doi: https://doi.org/10.3390/math8030360
54. *Kazim, M., Abbas, M., Hussain, S., Abbas, M. A.*, Fractional modelling of heat transfer through porous media for incompressible MHD fluid flow with Laplace transform approach, Partial Differ. Equ. Appl. Math. (2025) 101242. doi: https://doi.org/10.1016/j.padiff.2025.101242
55. *Yakubu, G., Abdulhameed, M., Adamu, G., Hassan, U., Kaurangini, M.*, Construction of the exact solution of blood flow of Oldroyd-B fluids through arteries with effects of fractional derivative, magnetic field and heat transfer, J. Mech. Med. Biol. **22** (2022) 2250068. doi: https://doi.org/10.1142/S0219519422500683
56. *Murad, A., Skauge, A., Skauge, T.*, Polymer retention leading to non-Darcy flow in porous media—influence of molecular weight, composition and mechanical degradation, Colloids Interfaces **10** (2026) 30. doi: https://doi.org/10.3390/colloids10020030
57. *Ray, A. K., Vasu, B., Murthy, P. V. S. N., Bég, O. A., Gorla, R. S. R., Kumar, B.*, Convective flow of non-homogeneous fluid conveying nano-sized particles with non-fourier thermal relaxation: Application in polymer coating, Arab. J. Sci. Eng. **47** (2021) 6559. doi: https://doi.org/10.1007/s13369-021-06467-w
58. *Nasir, M., Waqas, M., Kausar, M. S., Zamri, N., Bég, O. A.*, Cattaneo–Christov dual diffusive non-Newtonian nanoliquid flow featuring nonlinear convection, Chin. J. Phys. **89** (2024) 1164. doi: https://doi.org/10.1016/j.cjph.2022.05.005
59. *Tang, E., Tian, B., Fu, C.*, Apparent kinetic study of latex interpenetrating polymer networks poly(ethyl acrylate)/poly(styrene) and poly(styrene)/poly(ethyl acrylate) by two stages, Colloids Surf. A Physicochem. Eng. Asp. **333** (2009) 7. doi: https://doi.org/10.1016/j.colsurfa.2008.09.017
60. *Askar, S., Abouelregal, A. E., Marin, M., Foul, A.*, Photo-thermoelasticity heat transfer modeling with fractional differential actuators for stimulated nano-semiconductor media, Symmetry **15** (2023) 656. doi: https://doi.org/10.3390/sym15030656
61. *Turkyilmazoglu, M., Altanji, M.*, Fractional models of falling object with linear and quadratic frictional forces considering Caputo derivative, Chaos Solit. Fractals **166** (2023) 112980. doi: https://doi.org/10.1016/j.chaos.2022.112980
62. *Turkyilmazoglu, M.*, An efficient computational method for differential equations of fractional type, Comput. Model. Eng. Sci. **133** (2022) 47. doi: https://doi.org/10.32604/cmes.2022.020781
63. *Turkyilmazoglu, M.*, Hyperthermia therapy of cancerous tumor sitting in breast via analytical fractional model, Comput. Biol. Med. **164** (2023) 107271. doi: https://doi.org/10.1016/j.compbiomed.2023.107271